

**FORMULATION OF HIGHLY EXPOSED (001) FACET TITANIUM  
DIOXIDE/GRAPHENE OXIDE NANOCOMPOSITE FOR AN  
EFFICIENT PHOTODEGRADATION OF ORGANIC DYES**

**ARINI IZZATADDINI**

**FACULTY OF ENGINEERING  
UNIVERSITI MALAYA  
KUALA LUMPUR**

**2024**

FORMULATION OF HIGHLY EXPOSED (001) FACET TITANIUM  
DIOXIDE/GRAPHENE OXIDE NANOCOMPOSITE FOR AN  
EFFICIENT PHOTODEGRADATION OF ORGANIC DYES

ARINI IZZATADDINI

DISSERTATION SUBMITTED IN  
FULFILMENT OF THE  
REQUIREMENTS FOR THE DEGREE  
OF MASTER OF ENGINEERING SCIENCE

FACULTY OF ENGINEERING  
UNIVERSITI MALAYA  
KUALA LUMPUR

2024

UNIVERSITI MALAYA

## ORIGINAL LITERARY WORK DECLARATION

Name of Candidate : Arini Izzataddini  
Registration/Matric No : S2000899/1  
Name of Degree : Master of Engineering Science (M.Eng.Sc)  
Title of Thesis : “Formulation of Highly Exposed (001) Facet Titanium Dioxide/Graphene Oxide Nanocomposite for an Efficient Photodegradation of Organic Dyes.”  
Field of Study : Advanced Materials and Technology (NEC 524 : Chemical Process)

I do solemnly and sincerely declare that:

- (1) I am the sole author/writer of this work;
- (2) This work is original;
- (3) Any use of any work in which copyright exists was done by way of fair dealing and for permitted purposes, and any excerpt or extract from, or reference to, or reproduction of any copyright work has been disclosed expressly and sufficiently, and the title of the work and its authorship have been acknowledged in this work;
- (4) I do not have any actual knowledge, nor do I ought reasonably to know that the making of this work constitutes an infringement of any copyright work;
- (5) I hereby assign all and every rights in the copyright to this work to the University of Malaya (“UM”), who henceforth shall be the owner of the copyright in this work, and that any reproduction or use in any form or by any means whatsoever is prohibited without the written consent of UM having been first had and obtained;
- (6) I am fully aware that if in the course of making this work, I have infringed any copyright, whether intentionally or otherwise, I may be subject to legal action or any other action as may be determined by UM.

Candidate’s Signature

Date : 1<sup>st</sup> April 2024

Subscribed and solemnly declared before,  
Witness’s Signature

Witness’s Signature

Name:  
Designation:  
Date:

**[FORMULATION OF HIGHLY EXPOSED (001) FACET TITANIUM  
DIOXIDE/GRAPHENE OXIDE NANOCOMPOSITE FOR AN EFFICIENT  
PHOTODEGRADATION OF ORGANIC DYES]**

**ABSTRACT**

Photodegradation has been considered one of the most effective ways to remove organic dyes from wastewater. As one of the semiconductor materials, TiO<sub>2</sub> has shown tremendous potential due to its chemical stability and good photocatalytic efficiency. The catalysts' crystalline information, morphology, and optical properties were studied using Fourier Transform Infrared (FTIR), X-ray diffraction (XRD), Raman, TEM, and UV-visible absorption spectroscopy. In this research, the photocatalytic activity of five types of photocatalyst; TiO<sub>2</sub> P25, TiO<sub>2</sub> (001), Graphene Oxide (GO), TiO<sub>2</sub> P25/GO, and TiO<sub>2</sub> (001)/GO—was studied by the degradation of methylene blue, rhodamine b, crystal violet, and a mixture of the three dyes above in an aqueous medium under visible light and different contact time variations. This semiconductor/carbon composite material has excellent potential for removing organic stains and is applicable in water purification. The photocatalytic experiment showed that TiO<sub>2</sub> (001)/GO nanocomposites performed the highest photodegradation activity. The removal rates are 95%, 92%, 94%, and 87% for the photodegradation of methylene blue, rhodamine b, crystal violet, and a mix of the three dyes, respectively. It followed a pseudo-first-order kinetic model. The results indicated that TiO<sub>2</sub> (001)/GO nanocomposite is a highly efficient photocatalyst for removing persistent organic pollutants in water.

**Keywords:** Photocatalytic degradation, Nanocomposite, Organic dyes, TiO<sub>2</sub>, Graphene Oxide

**[RUMUSAN NANOKOMPOSIT TITANIUM DIOKSIDA/GRAFEN OKSIDA  
TERDEDAH TINGGI (001) UNTUK PENURUNAN FOTO YANG CEKAP  
PEWARNA ORGANIK]**

**ABSTRAK**

Photodegradation telah dianggap sebagai salah satu cara paling berkesan untuk membuang pewarna organik daripada air sisa. Sebagai salah satu bahan semikonduktor, TiO<sub>2</sub> telah menunjukkan potensi yang sangat besar kerana kestabilan kimianya dan kecekapan fotomangkin yang baik. Maklumat hablur, morfologi, dan sifat optik pemangkin dikaji menggunakan spektroskopi Inframerah Transformasi Fourier (FTIR), Difraksi Sinar-X (XRD), Raman, TEM, dan spektroskopi serapan UV-Visible. Dalam penyelidikan ini, aktiviti fotomangkin lima jenis fotomangkin; TiO<sub>2</sub> P25, TiO<sub>2</sub> (001), Graphene Oxide (GO), TiO<sub>2</sub> P25/GO, dan TiO<sub>2</sub> (001)/GO; telah dikaji oleh degradasi metilena biru, rhodamine b, kristal violet, dan campuran tiga pewarna yang dinyatakan dalam medium akueus di bawah cahaya yang boleh dilihat dan variasi masa sentuhan yang berbeza. Komposit bahan semikonduktor/karbon ini mempunyai potensi yang sangat baik dalam mengeluarkan pewarna organik dan boleh digunakan dalam penulenan air. Eksperimen fotokatalitik menunjukkan bahawa nanokomposit TiO<sub>2</sub> (001)/GO melakukan aktiviti fotodegradasi yang paling tinggi. Kadar penyingkiran ialah 95%, 92%, 94% dan 87% masing-masing untuk penguraian foto metilena biru, rhodamine b, ungu kristal, dan campuran ketiga-tiga pewarna itu. Ia mengikuti model kinetik *pseudo-first order*. Keputusan menunjukkan bahawa nanokomposit TiO<sub>2</sub> (001)/GO adalah fotomangkin yang sangat cekap untuk membuang bahan pencemar organik yang berterusan dalam air.

**Kata kunci :** Degradasi fotokatalitik, Nanokomposit, Pewarna organik, TiO<sub>2</sub>, Graphene Oxide

## ACKNOWLEDGEMENTS

With this opportunity, I would like to express my sincere thanks and gratitude to my supervisors, Associates Professor Dr Badrul Hisham Bin Mohamed Jan, Associate Professor Dr Munawar Khalil, and Dr Zulhelmi Bin Amir, for their valuable guidance, support, knowledge, and encouragement throughout the research. Their thorough attention to detail, acute yet constructive criticism, and insightful comments assisted me in shaping the path of this thesis research to the form presented here.

I would also like to thank all the Department of Chemical Engineering staff members at the University of Malaya and the Department of Chemistry University of Indonesia. Most importantly, all my colleagues and partners in Low Dimension Material Research Groups have helped me immensely in my research work.

I would also like to extend my eternal gratitude and love to my parents, brothers, sister, prominent families, and best friends for their love, endless support, and dedication to finishing my research smoothly.

Finally, I thank the FRGS program at the University of Malaya for providing the Research grant, the Department of Chemical Engineering at the University of Malaya, and the Department of Chemistry, University of Indonesia, for providing the facilities to take this project through in its entirety.

## TABLE OF CONTENT

<b>ORIGINAL LITERARY WORK DECLARATION</b> .....	<b>ii</b>
<b>ABSTRACT</b> .....	<b>iii</b>
<b>ABSTRAK</b> .....	<b>iv</b>
<b>ACKNOWLEDGEMENTS</b> .....	<b>v</b>
<b>TABLE OF CONTENT</b> .....	<b>vi</b>
<b>LIST OF FIGURES</b> .....	<b>viii</b>
<b>LIST OF TABLES</b> .....	<b>ix</b>
<b>LIST OF SYMBOLS AND ABBREVIATIONS</b> .....	<b>x</b>
<b>LIST OF APPENDICES</b> .....	<b>xii</b>
<b>CHAPTER 1: INTRODUCTION</b> .....	<b>1</b>
<b>CHAPTER 2: LITERATURE REVIEW</b> .....	<b>11</b>
2.1. Dye Pollution .....	11
2.2. Methylene Blue Dyes .....	12
2.3. Rhodamine B Dyes .....	13
2.4. Crystal Violet Dyes .....	14
2.5. Properties of TiO <sub>2</sub> .....	15
2.6. Crystal Facet Engineering .....	18
2.7. Graphene Oxide .....	19
2.8. TiO <sub>2</sub> /GO nanocomposite .....	22
2.9. Solvothermal Method .....	24
2.10 . Photocatalyst and Photocatalysis .....	25
2.11 . Mechanism of Photodegradation of Organic Dyes .....	31
2.12 . Pseudo First-Order Kinetics .....	33
2.13 . First-Order Kinetics .....	34
<b>CHAPTER 3: RESEARCH METHODOLOGY</b> .....	<b>35</b>
3.1. Place and Time .....	35
3.2. Materials and Chemical Compounds .....	35
3.2.1. Materials.....	35
3.2.2. Chemical Compounds .....	36
3.3. Synthesis of Graphene Oxide.....	36
3.4. Synthesis of TiO <sub>2</sub> nanosheets with (001) facet exposure.....	37
3.5. Synthesis of Graphene Oxide/TiO <sub>2</sub> Nanocomposite.....	37
3.6. Characterization .....	38

3.7. Photocatalytic Activity Studies .....	38
3.8. Analysis for measuring the dye concentration, degradation, and removal percentage.....	39
3.9. Kinetic Studies .....	40
<b>CHAPTER 4: RESULT AND DISCUSSION.....</b>	<b>41</b>
4.1. Synthesis of Graphene Oxide.....	41
4.2. Synthesis of TiO <sub>2</sub> (001) exposure using a solvothermal method.....	42
4.3. Evaluation of Photocatalytic Performances .....	63
4.4. Kinetic Studies of Photocatalytic Degradation .....	70
4.5. Possible Mechanism For Photocatalytic Performance .....	73
<b>CHAPTER 5: CONCLUSIONS.....</b>	<b>76</b>
<b>REFERENCES.....</b>	<b>77</b>
<b>List of Publications and Papers Presented .....</b>	<b>84</b>
<b>Appendix.....</b>	<b>87</b>



## LIST OF FIGURES

Figure 2. 1: Methylene Blue Structure .....	13
Figure 2. 2: Rhodamine B Structure .....	14
Figure 2. 3: Crystal Violet Structure .....	15
Figure 2. 4: TiO <sub>2</sub> (a) 101,(b) 001, and (c) 010 structures.....	18
Figure 2. 5: Graphene Oxide Structure .....	21
Figure 3. 1: Research Methodology Overview .....	35
Figure 4. 1: TBOT Chemical Structure.....	43
Figure 4. 2: The schematic role illustration of solvent and additives on the morphology control of crystal (001) and (101) facets. ....	44
Figure 4. 3: Fabrication of colloidal solution of exfoliated graphene nanosheets in water: ethanol solution using ultrasonic technology .....	47
Figure 4. 4: (a) XRD pattern, (b) FTIR spectra, and (c) Raman spectra of TiO <sub>2</sub> P25, TiO <sub>2</sub> (001), GO, TiO <sub>2</sub> P25/GO, and TiO <sub>2</sub> (001)/GO nanocomposites. ....	50
Figure 4. 5: TEM and HR-TEM image (inset: SAED) of (a,b) TiO <sub>2</sub> P <sub>25</sub> , (c,d) TiO <sub>2</sub> (001), (e,f) GO, and (g,h) TiO <sub>2</sub> (001)/GO nanocomposite.....	53
Figure 4. 6: Truncated Tetragonal Bypiramid Structure of TiO <sub>2</sub> .....	54
Figure 4. 7: Kubelka-Munk plot of photocatalysts .....	58
Figure 4. 8: DRS Spectra of as-prepared photocatalyst .....	59
Figure 4. 9: (a) Urbach Energy of TiO <sub>2</sub> (001) and TiO <sub>2</sub> (001)/GO, and (b) Urbach Energy of TiO <sub>2</sub> P25 and TiO <sub>2</sub> P25/GO nanocomposite. ....	60
Figure 4. 10: The absorbance spectra of dye compounds mixture.....	65
Figure 4. 11: Photodegradation efficiency and the plot of removal Ct/C0 of MB (a,e); RhB (b,f); CV (c,g); and Mix dyes (d,h).....	67
Figure 4. 12: Pseudo-first order kinetics of (a) MB, (b) RhB, (c) CV, and (d) Mix dyes and First order kinetic of (e) MB, (f) RhB, (g) CV, and (h) Mix dyes .....	71
Figure 4. 13: Proposed energy band diagram mechanism for photocatalytic degradation of TiO <sub>2</sub> (001)/GO nanocomposite dyes.....	73

## LIST OF TABLES

Table 2. 1: Chemical Properties of TiO <sub>2</sub> Anatase, Rutile, and Brookite .....	17
Table 2. 2: Photocatalytic activity of various TiO <sub>2</sub> /GO photocatalysts .....	30
Table 4. 1: TiO <sub>2</sub> (001) Facet exposure based on TEM and Raman spectroscopy analysis .....	58

Universiti Malaya

## LIST OF SYMBOLS AND ABBREVIATIONS

Symbol	Definition
Co	The initial concentration of dye
Ct	Concentration after time (t)
$K_{app}$ / K	The apparent first-order rate constant of the pseudo-first-order adsorption model
R <sup>2</sup>	Linear regression
t <sub>1/2</sub>	First-order reaction's half-life
e <sup>-</sup>	Electron pairs
h <sup>+</sup>	Positive holes

Abbreviation	Definition
POP	Persistent Organic Pollutants
TiO <sub>2</sub>	Titanium Dioxide
TiO <sub>2</sub> (001)	Titanium dioxide with 001 facets exposure
GO	Graphene Oxide
GO/TiO <sub>2</sub>	Graphene Oxide – Titanium dioxide nanocomposites
GO/TiO <sub>2</sub> (001)	Graphene Oxide – Titanium dioxide with 001 facets exposure nanocomposites
HF	Hydrofluoric Acid
H <sub>2</sub> O	water
H <sub>2</sub>	Hydrogen gas
O <sub>2</sub>	Oxygen gas
CO <sub>2</sub>	Carbon Dioxide
Pt	Platina metal
ClO <sub>2</sub>	Chlorine Dioxide
C <sub>2</sub> H <sub>5</sub> OH	Ethanol
C <sub>16</sub> H <sub>18</sub> N <sub>3</sub> SCl	The chemical formula of methylene blue
H <sub>2</sub> SO <sub>4</sub>	Sulfuric Acid
KMnO <sub>4</sub>	Pottasium Permanganate
H <sub>2</sub> O <sub>2</sub>	Hydrogen Peroxide
EG	Ethylene Glycol
MB	Methylene Blue
RhB	Rhodamine B
CV	Crystal Violet
NO <sub>2</sub>	Nitrogen Dioxide
N <sub>2</sub> O <sub>4</sub>	Dinitrogen Tetraoxide
Mn <sub>2</sub> O <sub>7</sub>	Manganese Heptoxide
HMnO <sub>4</sub>	Permanganic Acid
-COOH	Carboxyl
-OH	Hydroxy
-C-O-C	Epoxide
•OH	Hydroxy radical
VB	Valance Band
CB	Conduction Band
PCBs	Polychlorinated Biphenyls
AOP	Advance Oxidation Process

pH	Potential of Hydrogen
FTIR	Fourier Transform Infrared spectroscopy
TEM	Transmission Electron Microscopy
XRD	X-Ray Diffraction spectroscopy
UV	Ultraviolet
UV-Vis DRS	Ultraviolet-visible Diffuse Reflectance Spectroscopy
cm	centimeter
nm	nanometer
m	meter
mg	milligram
W	watt
TBOT	Titanium (IV) Butoxide
CCD	Charge-Coupled Devices
LED	Light Emitting Diode
hr	hour
SAED	Selected area diffraction
eV	Electron volt
TOB	Truncated Octahedral Bipyramid
L-H	Langmuir-Hinshelwood

## LIST OF APPENDICES

APPENDIX B	: Calculation of Band Gap Energy Values.....	87
APPENDIX C	: Calculation of interlayer spacing on the results of the XRD characterization of Graphene Oxide (GO).....	87
APPENDIX D	: Calculation of methylene blue, rhodamine b, and crystal violet calibration curve.....	88
APPENDIX E	: Calculation of calibration curve for a mixture of MB + RhB + CV dyes.....	89
APPENDIX F	: Methylene Blue photodegradation data using GO/TiO <sub>2</sub> (001).....	89
APPENDIX G	: Rhodamine B photodegradation data using GO/TiO <sub>2</sub> (001).....	90
APPENDIX H	: Crystal violet photodegradation data using GO/TiO <sub>2</sub> (001).....	90
APPENDIX I	: Photodegradation data of MB + RhB + CV dye mixtures using GO/TiO <sub>2</sub> (001).....	90

Universiti Malaysia

## CHAPTER 1: INTRODUCTION

In recent years, many organic residues have been discovered in various water systems, including streams, lakes, and other aquatic environments, particularly those near industrial facilities. Industries such as textile manufacturing, pharmaceuticals, and food and beverage production are notable sources of these organic pollutants (Sinar Mashuri et al., 2020). Among these pollutants, synthetic organic dyes primarily contribute to environmental deterioration (Sharif, 2020). It is estimated that textile production alone accounts for approximately 20% of worldwide water pollution stemming from dyeing and finishing processes. Furthermore, the textile industry significantly contributes to global greenhouse gas emissions, surpassing the combined emissions from international flights and maritime shipping.

Organic dyes are highly hazardous and persistent substances with significant chemical stability. These dyes may persist in the atmosphere for several days and remain in the soil for years. Furthermore, they are recognized and suspected carcinogens. Human health can be severely compromised by the toxicity of water-contaminated dyes, leading to conditions such as kidney dysfunction, as well as impacts on neurological and reproductive systems. Annually, approximately 3,575,000 people succumb to waterborne illnesses, with a disproportionate number being children. Water used in textile manufacturing may contain contaminants such as formaldehyde, chlorine, and heavy metal compounds. These pigments obstruct light penetration into the water, diminishing the efficiency of photosynthesis in aquatic plants and impeding their growth.

Methylene blue (MB), rhodamine B (RhB), and crystal violet (CV) dyes are continuously used in the textile industry. As the sources of blue, reddish-purple, and violet colours in textiles, these dyes are often found in aquatic ecosystems as hazardous waste. Excessive concentrations of these dyes in the water can disrupt the ecosystem. One is limiting the sun's rays from reaching marine life. Methylene blue (7-(dimethylamino)phenothiazin-3-ylidene]-dimethylammonium chloride) (MB) is commonly used as a dye source in cotton, wool, and paper. It is also used in the culinary, cosmetic, and pharmaceutical industries. MB dye has several uses in the pharmaceutical and medical industries, including tissue or lymphatic mapping during parathyroid surgery (Smithson & Mitchell, 2019).

However, the discharge of wastewater containing Methylene Blue dye from any of the industries mentioned above, whether partially or fully treated, could pose serious health risks (Oladoye et al., 2022). For instance, Methylene blue dye can potentially induce a range of human ailments, such as cyanosis, tissue necrosis, the development of Heinz bodies, vomiting, jaundice, shock, and elevated heart rate, among other conditions. Rhodamine B is also extensively used in textile colouration and is hardly distinguishable from methylene blue. Cytochrome P450 in the body breaks down the xenobiotic chemical rhodamine B to create free radicals (Sulistina & Martini, 2020). It alters the activity of superoxidase dismutase (SOD), which causes oxidative stress, damage, increased cell death, and brainstem dysfunction. Crystal violet is also accounted for as a significant class of commercial dyes. It has a variety of uses, including as a biological stain, veterinary medicine, dermatological agent, an additive in poultry feed to stop the spread of the fungus, mould, and intestinal parasites, textile dyeing, and paper printing (REHMAN et al., 2017).

Additionally, research findings showed that crystal violet dye is mutagenic, carcinogenic, and regarded as a biohazard agent (Mani & Bharagava, 2016).

Numerous methods have been studied on how to remove organic dye pollutants from water, such as adsorption, use of surfactants, oxidation, solvent extraction, filtration, reverse osmosis, ion exchange, chemical degradation, coagulating agents, and photodegradation (Pakade et al., 2011). Zeolite was used by Yagub et al. to adsorb various colours, metal ions, and phenols. However, because of its inadequate sorption capacity, it was ineffective in removing dyes. Additionally, the biological approach was selected as the preferred pathway for dye removal. This process falls short of removing harmful particles from textile dye effluent, which could lead to environmental dye resistance. As a result, appropriate dye treatment techniques with a high removal capability and the ability to refrain from creating any other dangerous materials ought to be offered.

Currently, photocatalytic degradation using photoactive materials is the most effective way to remove organic dyes from water. Especially among scientists, interest in the photodegradation of organic dyes has increased rapidly for the past ten years (Tang et al., 2003). Photocatalytic degradation has gained popularity as one of the most effective ways to remove persistent organic pollutants because of its convenience, harmlessness, and low cost. In 1972, Honda and Fujishima carried out the first photocatalytic degradation methods using  $\text{TiO}_2$ . It can be used to harvest solar energy and produce hydrogen fuel.

Since then, a keen interest has emerged in utilizing semiconductor materials as catalysts for photocatalytic removal. The presence of conjugation on the aromatic ring within organic dyes has been noted to facilitate more favorable photocatalytic reactions by creating an electron-rich environment for such processes (Zhao, Sheng, Chen, & Wang,



2012; Saeed, Muneer, Haq, & Akram, 2022). Moreover, the highly reactive hydroxyl radical ( $\text{OH}\bullet$ ) produced during photodegradation is crucial in eliminating dye waste. Metal oxides and sulfides like ZnO, CuS,  $\text{Fe}_2\text{O}_3$ , CdS, and  $\text{TiO}_2$  are commonly used semiconductor materials for photodegradation. Titanium dioxide ( $\text{TiO}_2$ ) is preferred among these semiconductors due to its chemical stability, biological and chemical inertness, cost-effectiveness, and exceptional photocatalytic efficiency.

Various methods such as sol-gel, hydrothermal, solvothermal, chemical vapor deposition (CVD), spray pyrolysis, electrodeposition, sonochemical, microwave, spin coating, and evaporation-induced self-assembly (EISA) are employed to synthesize  $\text{TiO}_2$  (Balasubramanian et al., 2004; Grätzel, 2001; Oshani et al., 2014; Su et al., 2004). Among these techniques, solvothermal synthesis offers several advantages over conventional methods, including enhanced uniformity, purity, and flexibility.

$\text{TiO}_2$ , a semiconductor with high stability and low toxicity, has gained interest in the photocatalyst field.  $\text{TiO}_2$  has three distinct crystalline stages: anatase, rutile, and brookite. Anatase and rutile have seen the most in-depth research, whereas brookite has less. When utilized as a photocatalyst, anatase  $\text{TiO}_2$  is the most active phase. Additionally, nanostructured  $\text{TiO}_2$ , including crystals, fibers, nanosheets, and nanotubes, is promising due to the increased photocatalytic activity from its vast surface areas. Although  $\text{TiO}_2$  has many advantages as a photocatalyst, its wide bandgap limits its ability to function outside the UV spectrum. Additionally, it results in a high rate of recombination for electron-hole pairs produced by photolysis, significantly reducing the photo efficiency of this oxide in photocatalytic processes. Numerous strategies must be developed to overcome the drawbacks.

According to Liu, Yu, & Jaroniec, 2011, the high surface energy of the (001) parts of anatase TiO<sub>2</sub> is a factor in their significant photocatalytic activity (S. Liu et al., 2011). The (001) facets of anatase TiO<sub>2</sub> have an average surface energy of 0.90 J m<sup>-2</sup>, much greater than the average surface energy of the TiO<sub>2</sub> 101 facets (0.44 J m<sup>-2</sup>) (Sajan et al., 2016). These factors greatly influence photodegradation's stability, adsorptive ability, and catalytic activity. The 100% unsaturated Ti<sub>5</sub>C atom and high surface energy of the (001) facets of anatase TiO<sub>2</sub> are also thought to contribute to their remarkable photocatalytic activity. These characteristics significantly impact photodegradation's stability, adsorptive capacity, and catalytic activity. In particular, the average surface energy of anatase. This discovery follows that of Bifen et al., who successfully used TiO<sub>2</sub> (001) doped TiOF<sub>2</sub> to degrade Rhodamine B dyes after 1 hour of visible light irradiation. The modified TiO<sub>2</sub> (001)/TiOF<sub>2</sub> with 66% degradation has twice as high degradation efficiency as commercial TiO<sub>2</sub> (Gao et al., 2015).

In addition to facet crystal modification, structure modification is also an effective method to increase the photocatalytic activity of titanium dioxide. The structural modification method uses a hollow or mesoporous structure with a large surface area to increase the adsorption ability of the reactants. Additionally, combining semiconductors with other materials has recently produced significant and promising results for eliminating dyes and enhancing the properties of semiconductors. There have been reports on several strategies, including metal/semiconductor, carbon/semiconductor, and semiconductor/semiconductor composites. Due to their sizeable visible light coverage and ability to slow down electron-hole recombination, carbonous material composites with semiconductors are among the most promising combinations (Sharma et al., 2018).

Graphene oxide stands out among carbonous materials due to its hydrophilic nature and ability to generate stable aqueous colloids through an easy and inexpensive solution. Since its large specific surface area makes it easier for  $\text{TiO}_2$  to be distributed, graphene oxide (GO) has received much attention as a material with great potential for and efficiency in improving the photocatalytic effectiveness of  $\text{TiO}_2$ . Furthermore, GO can act as an electronic transfer medium, slowing the rate at which electron-hole couples recombine. The narrow band gap will increase the pace at which electrons transfer charges. Organic contaminants like EDCs may be taken up through GO surface interactions. Thanks to its thin layer structure, GO exhibits excellent UV light transparency, enabling  $\text{TiO}_2$  to absorb UV light. GO would, therefore, significantly enhance  $\text{TiO}_2$  photocatalytic activity (Zhang et al., 2018)

Recently, there has been a surge in interest in GO/ $\text{TiO}_2$  nanocomposites for pollutant degradation. These nanocomposites, formed by integrating  $\text{TiO}_2$  with graphene or GO, offer several advantages over standalone  $\text{TiO}_2$ . They augment  $\text{TiO}_2$ 's adsorptive capacity by expanding its surface area and preventing electron-hole pairs' recombination by transferring photo-excited electrons to the surface of graphene or GO.

Therefore, in this research, the  $\text{TiO}_2$  (001)/GO nanoparticles are synthesized to obtain a new type of photocatalyst that can enhance the photocatalytic activity for dye removal and be suitable to work under visible light. The nanocomposite will also provide the facile synthesis process through the modified Hummer method. Using graphite flakes and TBOT as the raw material of this nanocomposite,  $\text{TiO}_2$  (001)/GO comes into sight as the photocatalyst that requires a relatively low cost, making this material more outstanding.

**Stage I** includes the preparation of the photocatalyst via the solvothermal method. Then, the TiO<sub>2</sub> nanoparticles were modified by exposing the surface to HF to increase the (001) exposure and by compositing TiO<sub>2</sub> with graphene oxide to improve solar light absorption and delay the recombination.

In this research, five types of photocatalysts were prepared:

- TiO<sub>2</sub> P25
- TiO<sub>2</sub> (001)
- Graphene Oxide
- TiO<sub>2</sub> P25/GO nanocomposite
- TiO<sub>2</sub> (001)/GO nanocomposite

**Stage II** involves determining the physicochemical properties of the photocatalyst by using Fourier-transformed infrared (FTIR) (Shimadzu IRPrestige-21), Raman spectroscopy, X-ray diffraction spectroscopy, a high-resolution transmission electron microscope (HR-TEM), and dynamic reflectance spectroscopy (DRS) instruments.

**Stage III** involves evaluating the photocatalytic activities of the as-prepared photocatalysts for the photodegradation of MB, RhB, and CV pollutants under LED light irradiation. The degradation products were subsequently analyzed using the UV-Vis spectrophotometer.

The research questions of this work are:

1. How are the characterizations of TiO<sub>2</sub> (001), Graphene Oxide (GO), TiO<sub>2</sub> P25/GO nanocomposite, and TiO<sub>2</sub> (001)/GO, and how do their properties compare?
2. Has the synthesis of the nanocomposite photocatalyst been effectively accomplished, demonstrating the integration of desired structural and compositional attributes?
3. What is the newly synthesized photocatalyst's band gap energy and its influence on the photocatalytic activity?
4. How much degradation is observed when removing methylene blue, rhodamine B, crystal violet, and mixed dye solutions treated with photocatalysts?
5. Which photocatalysts demonstrate superior efficacy in the degradation of organic dye solution?

The hypotheses of this study designed as follows:

1. The newly developed photocatalyst will exhibit distinct structural and compositional properties that can be observed through appropriate methods.
2. Nanocomposite synthesis will be successfully achieved with the desired structural and compositional features.
3. The band gap energy of the newly developed photocatalyst will decrease, leading to the advancement of photocatalytic properties.
4. The degree of degradation of photocatalysts will improve along with the significant degradation of organic dye solution.
5. TiO<sub>2</sub> (001)/GO nanocomposite will exhibit superior photocatalytic efficiency.

The objectives of this study are summarized as follows:

1. To **synthesize** the newly developed photocatalysts using appropriate methods, systematically observe and analyze their structural and compositional features.
2. To **characterize** TiO<sub>2</sub> (001), Graphene Oxide (GO), TiO<sub>2</sub> P25, TiO<sub>2</sub> P25/GO nanocomposite, and TiO<sub>2</sub> (001)/GO photocatalysts and compare their properties through comprehensive characterization techniques such as FTIR, XRD, Raman, and HR-TEM.
3. To **determine** the band gap energy of the newly synthesized photocatalyst using UV-DRS spectroscopy and Tauc plot analysis to understand its electronic structure and potential for photocatalytic activity.
4. To **quantify** the degradation efficiency of the photocatalysts by measuring the percentage degradation of methylene blue, rhodamine B, crystal violet, and mixed dye solutions under controlled experimental conditions, using UV-Vis spectrophotometry.
5. To **evaluate** the performance and efficiency of different photocatalysts in degrading organic dye solutions by analyzing the degradation kinetics, reaction rates, and degradation efficiency parameters to identify the photocatalyst(s) with superior performance.

This dissertation is structured into five chapters.

Chapter 1: Describe the contemporary environmental problem of water contamination, mainly using organic dyes and wastewater treatment. Along with the goals and scope of the work, the concept of wastewater treatment using TiO<sub>2</sub> and modified TiO<sub>2</sub> on MB, RhB, and CV dyes has been clearly described.

Chapter 2: The literature review and research background of wastewater treatment technology emphasize the mechanism of photocatalysis, TiO<sub>2</sub> photocatalysis, and the catalyst's modification and photocatalytic effectiveness in degrading dye pollutants.

Chapter 3: Define the formation of TiO<sub>2</sub> nanoparticles, their characterization, and the technique for modifying the TiO<sub>2</sub> surface and nanocomposite and using these photocatalysts to degrade MB, RhB, and CV.

Chapter 4: The characterization of synthesized TiO<sub>2</sub> nanoparticles, TiO<sub>2</sub> (001) nanoparticles, and TiO<sub>2</sub>/GO nanocomposites, as well as the photocatalytic activity of all synthesized photocatalysts toward the degradation of organic dyes, are presented, and discussed.

Chapter 5: Conclusions

## CHAPTER 2: LITERATURE REVIEW

### 2.1. Dye Pollution

Based on the Technical Policy on Prevention and Control of Wastewater Pollution Statistics in the Printing and Dyeing Industry, the textile sector is the sixth largest industrial wastewater discharger, releasing up to 900 million tons annually. The intricate dye complexes with aromatic rings bound to various functional groups with  $\pi$ -electron spectra may absorb light between 380 and 700 nm (Maheshwari et al., 2021). They produce colour because chromogens and chromophores are present.

Dyes exhibit a diverse array of complex structures. According to the third edition of the Dye Index, over 5,000 distinct dye variations with diverse chemical compositions, of which over 1,500 have been cataloged. Generally, dyes can be classified into eight groups based on their chemical structures: azo dyes, anthraquinone dyes, indigo dyes, phthalocyanine dyes, sulfur dyes, Jia Chuan dyes, triaryl methane dyes, and heterocyclic dyes. Furthermore, based on their application, dyes are typically categorized into fourteen main groups, including reactive dyes, acid dyes, direct dyes, insoluble azo dyes, vat dyes (referring to insoluble variants), soluble vat dyes, sulfur dyes, acid mordant dyes, medium acid dyes, oxidation dyes, polycondensation dyes, disperse dyes, basic dyes, cationic dyes, fluorescent dyes, and fluorescent brighteners (Ali et al., 2023). Additionally, neutral and cationic dyes are two distinct categories, separate from acid and alkaline dyes.

Textile dyes are highly toxic and potentially carcinogenic. It can remain in water for a long time due to the stability of thermal and light to resist biodegradation. The major environmental problem with dye absorption is its presence in bodies of water that absorb



and reflect the sun's rays. Excessive levels of textile dyes in water bodies disrupt the photosynthesis of aquatic plants or algae, as well as the ability of the receiving water to replenish itself with oxygen and absorb sunshine (Samchetshabam et al., 2017).

The refractory and xenobiotic properties of the dyes have adverse effects on the ecosystem's structure and functionality (Lellis et al., 2019). Particularly with long-term exposures, there can be significant effects on human health and aquatic biota, for instance. Another issue with a recalcitrant nature is that oxidative stress causes significant harm to plant growth and development, particularly photosynthesis and CO<sub>2</sub> assimilation (Lellis et al., 2019).

Humans and other mammals have crucial risks of being affected by textile dyes through oral ingestion or direct skin exposure. Once it gets into the human gut, the dye converts into toxic amino acids, which harm various tissues in human bodies.

Among the numerous varieties of dye, methylene blue (MB), rhodamine b (RhB), and crystal violet (CV) are the primary colouring agents utilized as blue, light purple, and violet colour sources.

## **2.2. Methylene Blue Dyes**

Methylene blue is a cationic thiazine dye that is widely used in the field of medicine to treat various illnesses and disorders. The chemical formula is C<sub>16</sub>H<sub>18</sub>N<sub>3</sub>SCl. Figure 2.1 shows the structure of the methylene blue. Due to its hydrophilic characteristics, complex aromatic structure, and remarkable resilience to light, temperature, and water, methylene blue cannot be destroyed through traditional water treatment techniques and can pollute the environment. The development of a methylene blue photodegradation process using

photocatalyst semiconductors and ultraviolet and visible light resulted from unsuccessful attempts to handle textile waste containing significant amounts of the chemical.

Methylene blue cannot be degraded through conventional water treatment processes because of its hydrophilic nature, complex aromatic structure, and high stability to light, temperature, and water, so it can cause environmental pollution. Wastewater treatment efforts for textiles, which contain a lot of methylene blue in the conventional way as adsorption shows less effective results, have developed a methylene blue photodegradation method using photocatalyst semiconductors and ultraviolet and visible light.

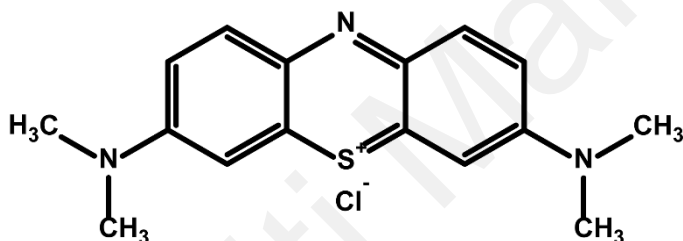


**Figure 2. 1: Methylene Blue Structure**

### 2.3. Rhodamine B Dyes

Besides methylene blue, rhodamine B (RhB) also gained interest as nature's most common persistent organic pollutant. Unlike other POPs, RhB is highly soluble in water. However, it can still cause considerable damage to humans and the environment if overexposed. It has  $C_{28}H_{31}N_2O_3Cl$  as its chemical formula. The structure of rhodamine b is displayed in Figure 2.2.

Rhodamine B contains a chlorine bond, a reactive and hazardous inorganic chemical. *Dye synthesis* is the process that binds chlorine ions. Triarylmethane and xentane are two colours that can be produced using the Friedl-Crafts reaction. Fluorescein is made via the

reaction of phthalic anhydride with resorcinol when zinc chloride is present. Rhodamine B will result from this reaction if resorcinol is substituted with N-N-diethylamino phenol.

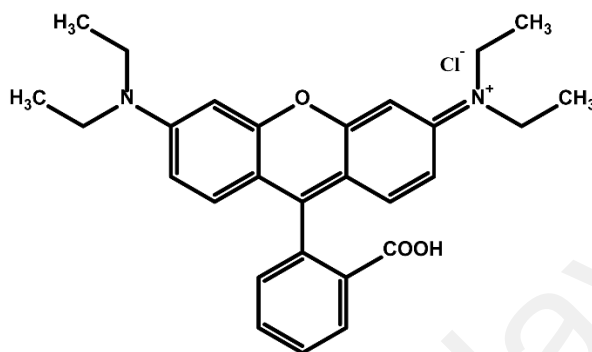


**Figure 2. 2: Rhodamine B Structure**

There are conjugate bonds in addition to the rhodamine B and chlorine bonds. Rhodamine B's conjugate bond is what gives rise to its red colour. The finding that chlorine and rhodamine B both provide similar risks leads to the conclusion that the chlorine atom in rhodamine B harms humans. Halogens are made up of chlorine, and due to the nature of halogens in organic compounds, they are poisonous and carcinogenic (Oyekanmi et al., 2019).

#### **2.4. Crystal Violet Dyes**

Crystal violet (Figure 2.3), gentian violet, or methyl violet is a triphenylmethane dye widely used as a histological stain in bacterial classification. Crystal violet's colour depends on the acidity of the solution. The dye is blue-violet after water dissolves and can change to yellow in very acidic conditions. Crystal violet (CV) is a textile and paper dye component of navy blue and black ink for printing, ball-point pens, and inkjet printers. It is sometimes used to colourize products such as fertilizer, antifreeze, detergent, and leather.

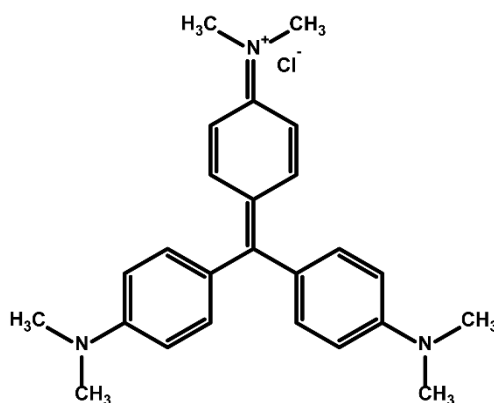


**Figure 2. 3: Crystal Violet Structure**

Despite having a wide range of applications, CV has been described as an environmentally toxic dye molecule that is recalcitrant and persists in the environment for a long time. It functions as a mitotic toxin, a potent carcinogen, and a powerful clastogenic, encouraging the growth of tumors (Mani & Bharagava, 2016). Therefore, in this study, we will examine the photocatalytic activity of an as-prepared photocatalyst on the photodegradation of methylene blue, rhodamine b, and crystal violet dyes.

## 2.5. Properties of TiO<sub>2</sub>

Titanium dioxide is an inorganic compound with the chemical formula TiO<sub>2</sub>. It is also known as titanium (IV) oxide or titania. Titanium exhibits octahedral geometry by being bonded to six oxide anions (Völz et al., 2006). Materials of different types and forms have shown massive ability due to their chemical stability, nontoxicity, and high reactivity (Schneider et al., 2014).

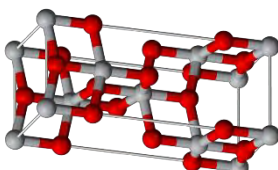
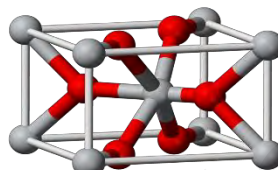
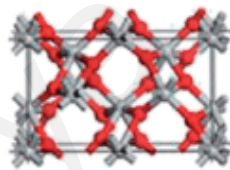
TiO<sub>2</sub> naturally occurs in three different forms: anatase, rutile, and brookite. The chemical properties of three different types of titanium dioxide are shown in Table 2.1. The characteristics of the bonds between Ti and O play significant roles in different TiO<sub>2</sub>

properties. Anatase crystalline has more active sites because of its higher surface area, much more than other crystal phases. The anatase phase has high separation activity. The concentration of oxygen vacancies on anatase nanoparticles is higher than on rutile nanoparticles. The larger bandgap of anatase also leads to a higher redox capability for the anatase form than the rutile form (Q. Guo et al., 2019)

80% of TiO<sub>2</sub> worldwide is used in paints, varnishes, paper, and plastics (Völz et al., 2006). However, over the past decades, the photocatalytic activity of TiO<sub>2</sub> has been massively discovered. TiO<sub>2</sub> has two influential bands: the valence band (VB) and the conduction band (CB). It mainly consists of Ti 3d and O 2p states at their band edges, respectively (Q. Guo et al., 2019).

Despite the advantages, TiO<sub>2</sub> has a significant drawback for the photocatalyst. TiO<sub>2</sub> has a large bandgap. The bandgaps of bulk anatase and rutile materials are 3.20 and 3.02 eV (equivalent to 384 and 410 nm, respectively) (Q. Guo et al., 2019). Titanium dioxide also only can absorb 5% of the light spectrum. This phenomenon leads to inadequate properties that work under visible light. That being said, it opens the room for improving the photocatalyst. Several approaches have been made to enhance the quality of TiO<sub>2</sub> as photocatalysts, such as commanding the surface structure of titanium dioxide and combining TiO<sub>2</sub> with other materials, such as other semiconductor materials, metal, or carbon compounds.

**Table 2. 1: Chemical Properties of TiO<sub>2</sub> Anatase, Rutile, and Brookite**

Properties	Anatase	Rutile	Brookite
<b>Crystal Structure</b>	 <p>Tetragonal</p>	 <p>Tetragonal</p>	 <p>Orthorhombic</p>
<b>Lattice constant (Å)</b>	$a=b=3.784$ $c=9.515$	$a=b=4.5936$ $c=2.9587$	$a=9.184$ $b=5.447$ $c=5.154$
<b>Density (g/cm<sup>3</sup>)</b>	3.79	4.13	3.99
<b>Ti-O bond length (Å)</b>	1.937 (4) 1.965 (2)	1.949 (4) 1.9980 (2)	1.87 to 2.04
<b>O-Ti-O bond angle</b>	77.7° 92.6°	81.2° 90.0°	77.0° to 105
<b>Reflective index</b>	2.56, 2.48	2.61, 2.90	2.58, 2.70
<b>The band gap (eV)</b>	3.05 to 3.23	2.98 to 3.02	3.1 to 3.4
<b>Application</b>	Photocatalyst	Solar cells, optics	Difficult to prepare

## 2.6. Crystal Facet Engineering

Among the ways to enhance the photocatalytic properties of  $\text{TiO}_2$ , controlling the surface structure of  $\text{TiO}_2$  by chemical processes under nonequilibrium conditions is one solution to  $\text{TiO}_2$  drawbacks. Facet engineering is the technique used to control the surface exposure of  $\text{TiO}_2$  anatase, especially on planes. It allows the modification of the catalytic and physicochemical properties of  $\text{TiO}_2$  to be suitable for specific applications. One method to control surface exposure is using different crystal faces, specifically 001, 101, and 110 facet exposure. Each face has a different highlighted side, as shown in Figure 2.4.

By manipulating the synthesis conditions such as acidity, temperature, and precursor concentration, different crystal facets of  $\text{TiO}_2$  can be selectively exposed. In this case, high-pH and low-temperature synthesis processes can be employed to increase the exposure of  $\text{TiO}_2$  (001) facets.

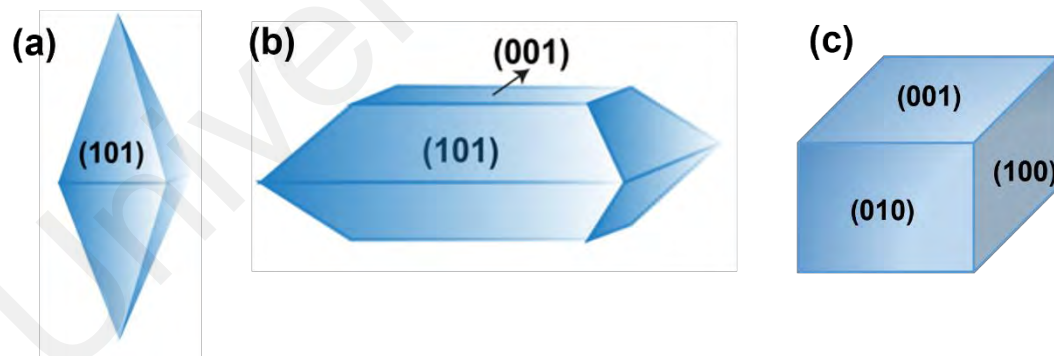


**Figure 2. 4:  $\text{TiO}_2$  (a) 101,(b) 001, and (c) 010 structures**

Amidst all the  $\text{TiO}_2$  facet exposure,  $\text{TiO}_2$  (001) is receiving much attention ascribed to its intriguing physicochemical characteristics, including active and high-surface-energy unsaturated Ti atoms. Various techniques are used to prepare titanium dioxide, and typically facets are used as a capping agent to restrict the formation of the more reactive

(001) catalytic aspect (Kusiak-nejman & Morawski, 2019). Research on the photocatalysis of TiO<sub>2</sub> anatase with high (001) facet exposure has concentrated chiefly on the high energy of the facet (001) in the liquid phase photodegradation of organic contaminants.

Due to their high surface energy and 100% unsaturated Ti<sub>5</sub>C atoms, the 001 facets of anatase TiO<sub>2</sub> are thought to exhibit solid photocatalytic activity. These characteristics significantly influence the photocatalyst's stability, adsorptive capacity, and catalytic activity. For example, the average surface energy of anatase TiO<sub>2</sub> for the 001 facets is 0.90 J<sub>amV</sub><sup>2</sup>, which is significantly higher than that for the 101 facets (0.44 J<sub>amV</sub><sup>2</sup>).

Several approaches have been conducted to obtain the (001) facets exposure. Yang et al. prepared the TiO<sub>2</sub> highly exposed (001) using a solvothermal synthetic route. The synergistic function of propanol and HF solution reveals that they can strengthen the stabilization and stimulate the preferred growth (Yang et al., 2008). On the other hand, Ye et al. successfully obtained 90% exposure to TiO<sub>2</sub> anatase using potassium titanate without fluorine or organic compounds (Ye et al., 2013). In this study, the (001) facets were exposed using solvothermal by reacting titanium butoxide and hydrofluoric acid solutions to obtain uniformity and purity.

## 2.7. Graphene Oxide

Graphene oxide is a layered carbon structure with functional groups comprising oxygen (=O, -OH, -O-, -COOH) bonded to the layer's edges and two opposite sites. Graphene oxide can exist as a monolayer or multilayer material. GO (graphene oxide) monolayer is a structure with one layer; two layers of graphene oxide are known as two-layered GO. In addition, if the layer is more than two and fewer than five, the material is referred to as few-layered graphene oxide. Lastly, the GO with two to ten layers is called multilayered GO,



and the material with more than eleven layers is intended as graphite oxide (Jiříčková et al., 2022).

Graphene oxide can be obtained by oxidizing graphene into graphite oxide, followed by the exfoliation of the multilayer graphite oxide into monolayer graphene oxide. Several different kinds of synthesis methods have been studied. The structure and properties of the materials strongly depend on graphene oxide fabrication methods. It will increase the number of oxygen-containing groups. Since graphene oxide is a very hydrophilic material, it is relatively simple to prepare a water- or organic solvent-based suspension (Jiříčková et al., 2022).

The structure model of graphene oxide has been discovered for decades. One of the most famous models is from Lerf and Kinowski in 1998. Aromatic groups, epoxide, and double bonds mainly build graphene oxide materials (Figure 2.5). The oxygen functional groups are attached to the upper and lower parts of the monolayer. It caused the creation of two layers of material with various concentrations. It mainly consists of epoxide and hydroxyl groups. The functional groups, including aromatic bodies, oxidized rings, and epoxides, are randomly distributed across the monolayer. Hydroxyl and carboxyl groups also influence the acidity level of graphene oxide. This model is the most acceptable and widely used among other graphene oxide models.

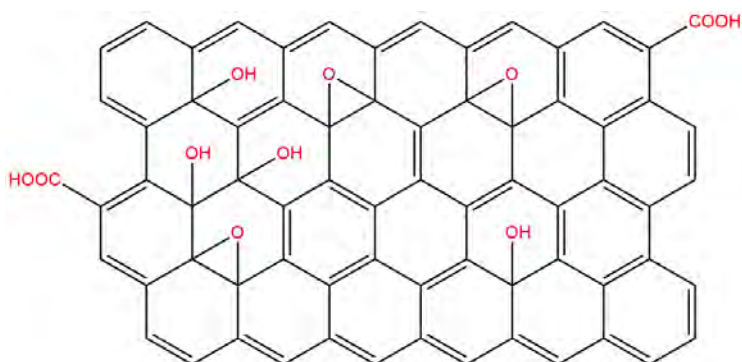


**Figure 2. 5: Graphene Oxide Structure**

This research synthesized graphene oxide using the modified Hummer method from graphite flakes. The main point of the Hummer method is the role of sulfuric acid as the solvent and, potassium permanganate and sodium nitrate as the oxidants. The Hummers method is a simple and fast method to synthesize graphene oxide. Despite the convenience of the methodology, it can lead to some disadvantages, such as the formation of toxic gases ( $\text{NO}_2$ ,  $\text{N}_2\text{O}_4$ , and  $\text{ClO}_2$ ) that can be explosives and incomplete oxidation results. A few alterations have been made with different strategies.

With the corresponding adjustment, graphene oxide was made using the following process: The temperature was kept at  $0\text{ }^\circ\text{C}$  to prevent overheating and explosions while adding other materials. The fundamental chemical reaction in the Hummers Method is the oxidation of graphite, presenting oxygen to carbon graphene. The oxidation occurs between the graphene and sulfuric acid as the solvent. Sulfuric acid significantly impacted the intercalation process from graphite flakes to graphene oxide. Intercalation is the process by which ions or molecules appear between the layered materials. Potassium permanganate is the oxidizing agent, and sodium nitrate is the catalyst, which also plays a vital role in this synthesis. The solution turned black after graphite and sodium nitrate were added. Kalium permanganate was added carefully by keeping the temperature below  $20^\circ\text{C}$ . Potassium permanganate reacts to form manganese heptoxide ( $\text{Mn}_2\text{O}_7$ ).  $\text{Mn}_2\text{O}_7$  is an active compound

in graphene oxidation. Other species, like the permanganate ion, may also contain excess and play a role in the reaction. The oxidant compounds have access to fill the space in the graphene layers.

In this research, graphene oxide will be used to enhance the photodegradation of  $\text{TiO}_2$  (001). Graphene oxide was chosen because it can enhance photocatalytic activity, improve light harvesting, facilitate electron transfer, prevent semiconductor aggregation, and improve stability and recyclability (P. Singh et al., 2020).

## **2.8. $\text{TiO}_2/\text{GO}$ nanocomposite**

To optimize the material's properties and function, many researchers focus on consolidating two types of materials to obtain a more outstanding characteristic. Several types of nanocomposites have been employed for the photodegradation of organic dyes.

Nanocomposites are materials with a solid structure where the distance between the phases is leastwise, constituting a dimension. Studies like the composite of metal/semiconductor, semiconductor/graphene oxide, and semiconductor/semiconductor have circulated for the past decades.

Among the often employed nanocomposites are carbon nanotube-based nanocomposites. Carbon nanotubes (CNTs) are desirable for nanocomposite materials due to their high surface area, superior electrical conductivity, and outstanding mechanical strength. CNT-based nanocomposites may effectively separate charges and encourage dye degradation under light irradiation when coupled with semiconductors (Giovannetti et al., 2017).

The second nanocomposite is based on metal oxide nanoparticles. Iron oxide ( $\text{Fe}_2\text{O}_3$ ), zinc oxide (ZnO), and titanium dioxide ( $\text{TiO}_2$ ) are examples of metal oxide nanoparticles that are frequently employed as photocatalysts for dye degradation. Adding these

nanoparticles to nanocomposites containing other materials (such as graphene or carbon nanotubes) can improve their photocatalytic efficiency by enhancing light absorption, charge transfer kinetics, and stability.

Polymer-based nanocomposites and hybrid nanocomposites are also the choices for nanocomposites. Nanocomposites for dye degradation can be created by loading polymer matrices with carbonaceous materials or semiconductor nanoparticles. Polymers allow flexibility in design and functionalization to customize the features of the nanocomposite for particular applications, in addition to providing a stable scaffold for the dispersion and immobilization of the photocatalytic components.

Graphene-TiO<sub>2</sub> and carbon nanotube-ZnO are two examples of hybrid nanocomposites that mix two or more nanomaterials to maximize each component's benefits. Compared to the individual components alone, these hybrid systems frequently show synergistic effects that improve photocatalytic activity, stability, and recyclability. Additionally, Graphene and its derivatives, such as graphene oxide (GO) and reduced graphene oxide (rGO), are frequently added to semiconductor matrices (such as TiO<sub>2</sub> and ZnO) to create graphene-based nanocomposites. Because graphene sheets and semiconductor nanoparticles work together synergistically, these graphene-based nanocomposites have increased photocatalytic activity (E. Singh & Nalwa, 2015).

These nanocomposites can be adjusted and optimized based on the particulars of the photodegradation process, such as the target dye molecules, light source, and environmental factors. Furthermore, the selection of nanomaterials and synthesis techniques significantly influences the functionality and suitability of the nanocomposite catalysts.

Integrating carbon materials with metal oxides has been reported to enhance semiconductor surface properties, narrow the band gap, and shift the energy absorption

band from the ultraviolet area to the visible light range. The combination of semiconductor and carbon materials is one of the most promising materials, especially for photodegradation, since it has extensive coverage of visible light and hinders hole recombination, including the nanocomposites of graphene oxide and  $\text{TiO}_2$  (Sharma et al., 2018). Literature reports several methods of synthesizing GO/ $\text{TiO}_2$  nanocomposites, such as sol-gel, electrochemical deposition, physical mixing, and hydrothermal methods (Khan et al., 2019).

The carbon element in GO will be doped. By replacing Ti atoms and establishing C-O or C=O bonds, carbon is introduced into the lattice from  $\text{TiO}_2$ , enhancing the efficacy of the photocatalytic reaction. These hybrid orbitals are created just below the  $\text{TiO}_2$  conduction band.

The suitable energy level of  $\text{TiO}_2$  transforms when graphene and  $\text{TiO}_2$  are combined to form a nanocomposite, and electrons then transmute the conduction band of  $\text{TiO}_2$  into the energy level of graphene. In addition to improving the adsorption of reactants in the visible range, the  $\text{TiO}_2$ /GO nanocomposites also facilitate the transfer and separation of charges (Zhou et al., 2021).

These nanocomposites display four outstanding attributes: pollutant adsorption capabilities, elongating the light absorption range, efficient charge transportation, and charge separation capabilities (Khan et al., 2019). GO/ $\text{TiO}_2$  nanocomposites were used for hydrogen fabrication, hydrogen storage, sensors, and photocatalytic degradation of dyes (Ahmed et al., 2019).

## **2.9. Solvothermal Method**

The solvothermal method is one of the preferred options for acquiring nanoparticles with diverse morphologies, properties, and simple techniques. Solvothermal synthesis creates

nanomaterials by utilizing a solvent at high pressures and temperatures (100–1000 °C and 1–10,000 atm, respectively). The procedure is typically carried out in a sealed vessel (such as an autoclave) close to or above the boiling point of the reaction medium. Chemical inertness is required for the reaction vessels. In the sealed autoclave, high pressure is created by heating the reaction solution above the solvent's boiling point. Under these circumstances, the solvent transforms into a supercritical fluid (a fluid in which the gaseous and liquid phases coexist). The autoclave's temperature is lowered until it reaches room temperature, which is when the reaction is complete. Solvents and other impurities are then removed. Adjusting the reaction temperature, precursor concentration, and reaction time has been used to create nanoparticles in various shapes, including spheres, rods, and tetrapods.

Furthermore, throughout this study, the nanocomposites of TiO<sub>2</sub> and GO were achieved via ultrasonic. The ultrasonic path was chosen to achieve maximum graphene oxide shell exfoliation. Graphene oxide (GO) possesses hydrophilic characteristics. Graphene oxide (GO) is made up of graphene sheets with carboxylic groups (COOH) on the edges, epoxide groups (-C-O-C), and hydroxyl groups (-OH) on the base plane. Electrostatic repulsion between the sheets can come from the ionization of the COOH edge group. This method enables the sheet to create water-borne suspended dispersions.

## **2.10. Photocatalyst and Photocatalysis**

A photocatalyst is a substance that absorbs light to increase its energy level and then transfers it to a reactant to cause a chemical reaction (Oshida, 2013). Photocatalysts are outstanding substances that can quickly transform solar energy for use in oxidation and reduction processes. Photocatalysts are employed in several applications, including

removing contaminants from water and the air, water splitting to produce H<sub>2</sub>, odor control, the inactivation of bacteria and cancer cells, and managing odor. The ability of photocatalyst materials to remove harmful and poisonous substances from the environment has generated much interest during the past ten years (Ghasemi, 2022).

Fujishima and Honda's groundbreaking research from 1972 demonstrated the viability of water splitting utilizing a straightforward electrochemical cell supported by a TiO<sub>2</sub> semiconductor configuration. It has dramatically sparked researchers' interest in using metal oxides in the energy sector. Since then, much research on semiconductors has been conducted on materials including TiO<sub>2</sub>, ZnO, and even C<sub>3</sub>N<sub>4</sub> for use in the production of H<sub>2</sub> and CH<sub>4</sub>, water and air purification, and solar cells. The term photocatalysis comes from combining the words 'photo' and 'catalysis.' Catalysis accelerates the reaction rate in a material by lowering the activation energy without affecting the result of the reaction.

Meanwhile, photocatalysis is a catalytic process that is carried out with the help of light irradiation. In photocatalysis, the material that acts as a catalyst is called a photocatalyst. The photocatalyst is a material that can accelerate the reaction rate with the help of light rays.

The photocatalyst technique's mechanism is widely known and divided into dye sensitization (charge injections), indirect dye removal (redox), and direct photolysis of dyes. The dye sensitization mechanism started with the absorption of photons. The energy should be equal to or greater than the band gap energy. It is followed by the excitation from the valence band to the conduction band that leads to pairing electrons and positive hole (h<sup>+</sup> and e<sup>-</sup>) formation. Then, the positive hole electron produces exciting dye (Dye\*) that

causes the unstable dye\* to transform into dye<sup>-</sup> or dye<sup>+</sup> radicals. The dyes spontaneously decompose into inorganic molecules (Saeed et al., 2022).

The indirect mechanism started with the absorption of photons. It must be noted that the photon's energy should be equal to or greater than the band gap. Afterward, the excitation from the valence band to the conduction band happened accordingly. It is followed by forming pairs of electrons and positive holes (h<sup>+</sup> and e<sup>-</sup>). The positive hole will react with electrons and undergo a series of reactions to produce hydroxyl radicals. The leading actor is hydroxyl radicals since they have non-solid selective oxidizing agent ability and will degrade organic pollutants. Photodegradation of dyes is affected by several factors, such as the concentration of dyes, pH conditions, the amount of catalyst, light intensity, and intermediate species. Photocatalyst conditions must be adjusted according to the desired result. Photodegradation of dyes is affected by several factors, such as the concentration of dyes, pH conditions, the amount of catalyst, light intensity, and intermediate species. Photocatalyst conditions must be adjusted according to the desired result.

Photocatalysts can be classified as homogeneous or heterogeneous depending on the employed catalyst. The reactants and the photocatalysts are in the same phase during homogeneous photocatalysis. The catalyst unit in homogeneous photocatalysis is a dissolved homogeneous molecule that can absorb light at specific wavelengths and has catalytic sites for oxidation and reduction reactions. Transition metal complexes have been widely used as catalysts in homogeneous photocatalysis. The photo-Fenton systems (Fe<sup>+</sup> and Fe<sup>+</sup>/H<sub>2</sub>O<sub>2</sub>) and ozone are the most often employed homogeneous photocatalysts. The reactive species is OH, a free radical that serves various functions.



Nevertheless, this photocatalyst has several drawbacks. Due to its intrinsic chemical features, this type of photocatalyst is susceptible to deactivation, which might limit its photocatalytic activity. Furthermore, it can only absorb a certain amount of the sun's rays. The photocatalyst's reusability is also impractical because of its solubility properties.

On the other hand, the catalyst and the reactants are in separate phases during heterogeneous catalysis. The most prevalent heterogeneous photocatalyst is a semiconductor, which has distinct properties. In the heterogeneous photocatalyst, the electrons are excited from the valence band (VB) to the conduction band (CB) after the sunbeam strikes the suspended catalyst, forming electron-hole pairs. These electron-hole pairs aid the electrocatalytic reduction and oxidation reactions as they travel to the surface. In this case, the surface of the photocatalyst is where the light-induced change occurs. Heterogeneous photocatalysis is preferred over homogeneous photocatalysis for wastewater treatment and sustainable energy.

For decades, pros and cons have been encountered to meet the desired effective photocatalyst to eradicate the organic compounds in water. The condition and dye pollution level determines which photocatalysts are utilized. Within this study, a photocatalyst is the primary material to remove the organic dyes from water. Nanocomposites between  $\text{TiO}_2$  (001) and GO are expected to reduce dye pollution effectively. Various standards and techniques are employed to assess the effectiveness of dye degradation in photocatalytic reactions. The degradation percentage, also known as efficiency, is widely used as a reference point determined by calculating the drop in dye concentration over a given time frame. However, some variables, including the type of dye, its initial concentration, the photocatalyst employed, and the reaction circumstances, might affect what is considered "efficient" degradation.

In photocatalytic dye degradation experiments, a degradation efficiency of 80% -90% or more is typically regarded as outstanding or highly efficient (Li et al., 2018). Nevertheless, it is imperative to consider the particular environment and prerequisites of any application. For example, regulatory standards may specify the lowest allowable degradation efficiency in wastewater treatment or environmental remediation. It is critical to compare results within the context of comparable experimental settings and procedures because benchmark values for efficient degradation may differ between research and applications. In addition to providing commentaries on the significance of their findings in the larger context of photocatalytic dye degradation research, researchers frequently offer extensive characterization data.

The efficiency of degradation of  $\text{TiO}_2$  (001)/GO nanocomposites compared with other similar photocatalysts is reported in the literature, and the results are listed in Table 2.2. It shows that the efficiency of photodegradation using the nanocomposite of graphene and  $\text{TiO}_2$  varies based on the material, dye solution, and condition during the removal.

More studies are being done to investigate and clarify the variables affecting  $\text{TiO}_2$  (001)/GO nanocomposites' dye degradation efficiency. Through an analysis of diverse synthesis techniques, compositional adjustments, and experimental setups, these investigations offer significant perspectives for enhancing the efficacy of GO/ $\text{TiO}_2$  nanocomposites in environmental remediation scenarios.

**Table 2. 2: Photocatalytic activity of various TiO<sub>2</sub>/GO photocatalysts**

Material	Dye Solution	Light Source	Irradiation Time	Efficiency	References
RGO/TiO <sub>2</sub> (001)	Basic Violet (BV)	LED Lamp	2.5 hr	60.2%	(H. Liu et al., 2018)
TiO <sub>2</sub> (001)/GO	Tartrazine	Solar Irradiation	240 min	63%	(Ramos et al., 2020)
Graphene Sheets/ TiO <sub>2</sub> (001)	Methylene Blue	500 W Xe Lamp	90 min	70%	(B. Liu et al., 2012)
GO/TiO <sub>2</sub>	Methyl Orange (MO)	48 W UV Lamp	4 hr	85.62%	(Lin et al., 2020)

## 2.11. Mechanism of Photodegradation of Organic Dyes

The specific mechanism of photocatalytic degradation of organic dyes starts with the excitation of electrons from the valence band (VB) to the conduction band (CB) after exposure to an incident photon, as shown in Figure 2.6. After the excitation, the existence of electron-hole pairs forms two potential outcomes. It may recombine to generate thermal energy or spread to the photocatalyst surface and react with the absorbed molecules. The photoexcitation of electrons and holes produced reactive radicals such as superoxide radicals ( $O_2^-$ ) and hydroxyl radicals ( $OH^-$ ). Furthermore, superoxide radicals ( $\bullet O_2^-$ ) can also be generated from the photosensitization of the organic dyes, leading to electron enhancement in the photocatalyst. These reactive species can swiftly and non-selectively break down organic contaminants.

In addition, several variables, such as the temperature, irradiation intensity, acidity of the solution, and the concentration of organic dyes, affect the effectiveness and selectivity of the photocatalytic degradation process. The organic dye molecules' protonation state and the surface charge of the photocatalyst are determined by the pH of the solution, which in turn influences the organic dye molecules' adsorption and eventual degradation. Increased dye adsorption onto the photocatalyst surface due to higher dye concentrations may speed up degradation but also raise the possibility of electron-hole pair recombination. Higher temperatures often accelerate the photocatalytic degradation rate due to greater molecular mobility and reaction rates. Temperature also affects the kinetics of the degradation events. Furthermore, the degree of electron excitation and the production of reactive species are determined by the intensity and wavelength of the incident light source, which impacts the overall efficiency of dye degradation.

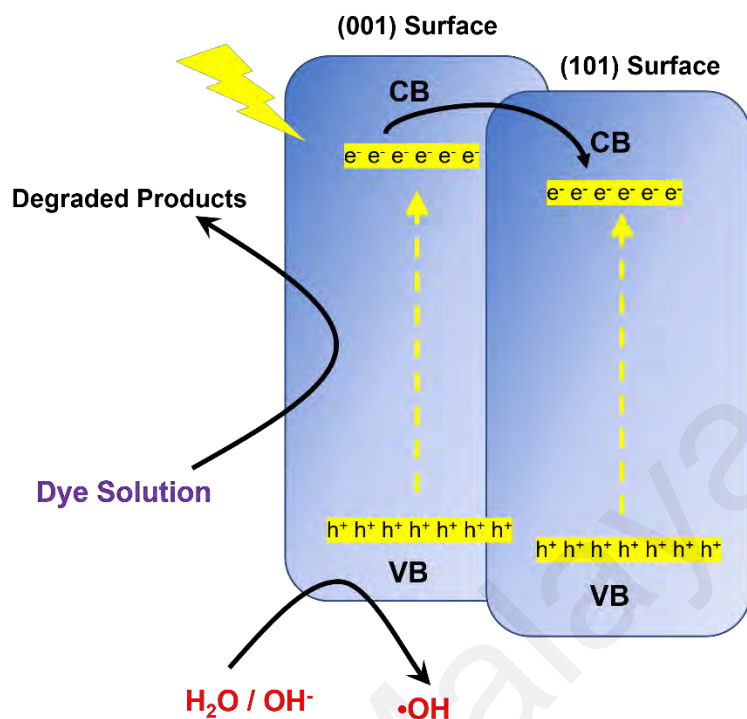


**Figure 2. 6: Proposed Mechanism for Photocatalytic Degradation**

The particular chemistry and characteristics of the organic dye molecules also significantly impact the kinetics and mechanism of degradation. Functional groups, conjugation, aromaticity, and other variables affect how reactive dye molecules are to reactive radicals and how sensitive they are to degradation pathways. Furthermore, by scavenging reactive radicals or interfering with surface reactions, coexisting pollutants or competing reactive species in the solution can impact the degradation efficiency. In conclusion, maximizing the process's efficiency and selectivity requires a thorough understanding of the precise mechanism underlying the photocatalytic degradation of organic dyes.

## 2.12. Pseudo First-Order Kinetics

The Langmuir-Hinshelwood isotherm model is usually considered to quantify the activity of heterogeneous photocatalysts. The equation is shown in Equation (1)

$$-\frac{dc}{dt} = \frac{kKC}{1 + KC'} \quad (1)$$

Where K and k are the thermodynamic adsorption constant and photodegradation rate constant, respectively. The term 'pseudo' indicates the reaction rate and is used as the prefix. In pseudo-first-order degradation, the photocatalysts, as one of the reactants, have a constant concentration, simplifying reaction kinetics.

Pseudo-first-order kinetics are obtained when the organic dye has a low concentration. The equation is valid by assuming that the activator of the degradation is steadily proportional to the concentration of dye molecules (Equation 2).

$$-\frac{dC}{dt} = k_1C, \quad (2)$$

Where  $k_1$  is the first-order reaction constant. The result of integrating the equation with the two boundary conditions is

$$\ln \frac{C_0}{C} = k_1 t \quad (3)$$

$$t_{1/2} = \frac{\ln 2}{k} = \frac{0.6932}{k} \quad (4)$$

The plot of  $\ln(C_0/C)$  vs. irradiation duration, as shown in Equation 3, where the slope represents the rate constant of photodegradation, can determine the linear zone. The most popular model for the complete photodegradation process is pseudo-first-order kinetics.

Here, Equation (4) is used to get the half-life. The first-order  $t_{1/2}$  model does not depend on the concentration of dyes.

### 2.13. First-Order Kinetics

A first-order reaction is a chemical process where the reaction rate depends linearly on the concentration of just one component. In other terms, a first-order reaction is a chemical reaction in which only one of the reactants' concentrations changes, and the rate of the reaction changes as a result. The value of a rate-constant response can be determined empirically using integrated rate equations. In such reactions, the reaction rate doubles if the concentration of the first-order reactant increases. Similarly, a five-fold increase in the concentration of the first-order reactant will result in a 500% increase in the reaction rate. The differential rate rule for the first-order reaction must be rearranged, as can be seen in Equation 5, to get the necessary form of the rate expression:

$$-\frac{dC}{dt} = kC \quad (5)$$

The integrated rate equation for a first-order reaction is shown in Equation 6 below,

$$C = C_0 e^{-kt} \quad (6)$$

Where  $C$  is the current concentration of the first-order reactant,  $C_0$  is the initial concentration of the first-order reactant,  $t$  is the time elapsed since the reaction began,  $k$  is the rate constant of the first-order reaction, and  $e$  is Euler's number (which is the base of the natural logarithm).

## CHAPTER 3: RESEARCH METHODOLOGY

### 3.1. Place and Time

This research was conducted at the Research Laboratory of the Department of Chemistry, University of Indonesia, University Faculty of Mathematics and Natural Sciences Indonesia, Depok, West Java, Indonesia, from January 2021 to September 2022.

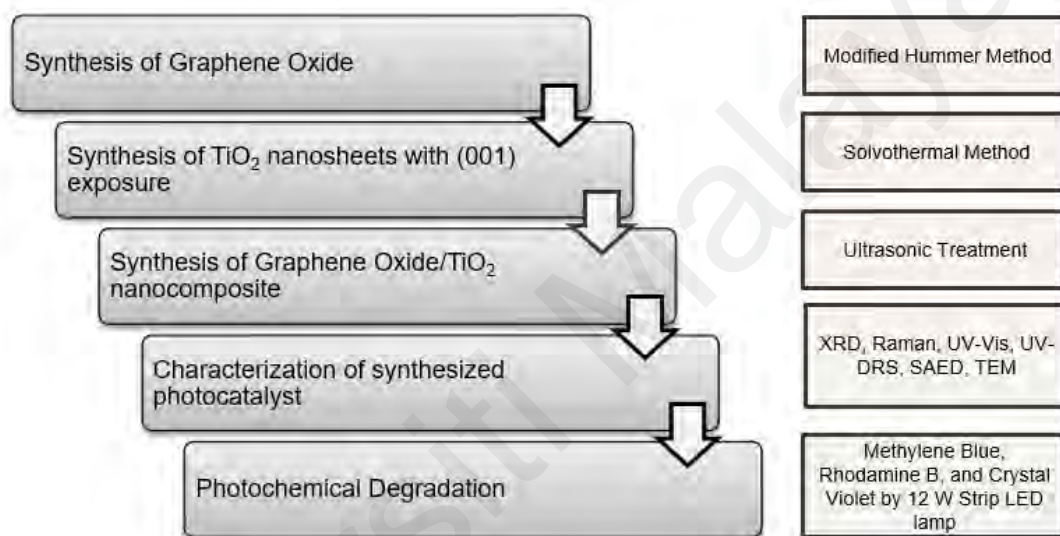


Figure 3. 1: Research Methodology Overview

### 3.2. Materials and Chemical Compounds

#### 3.2.1. Materials

Materials used in this study are chemical glass materials, a magnetic stirrer, a furnace, a Teflon-lined autoclave, a digital ultrasonic cleaner, a centrifuge (Hettich EBA-20 benchtop), an oven, weight scales, a mortar and pestle, a pH paper universal indicator, a digital pH meter, and LED strips lamp Phillips 12 watt.



The spectroscopy instruments used in this study are Transmission Electron Microscopy (TECNAI G2 Spirit Twin High-Resolution, USA), X-ray diffraction (Aerich Benchtop X-ray Diffractometer, Malvern Pananalytical, UK), Fourier Transform Infrared Spectroscopy (IRPrestige-21 Shimadzu, US), UV-Vis (Shimadzu UV-2450, US), UV-DRS, and Raman spectroscopy (iHR320 Modular Raman, France).

### **3.2.2. Chemical Compounds**

The chemical compounds used in this research are graphite flakes, sodium nitrate ( $\text{NaNO}_3$ ) (purity: 99.0%), potassium permanganate ( $\text{KMnO}_4$ ), hydrogen peroxide ( $\text{H}_2\text{O}_2$ ) (purity: 30%), hydrochloric acid ( $\text{HCl}$ , 37%), and sulfuric acid ( $\text{H}_2\text{SO}_4$ , 98%), which were purchased from Sigma-Aldrich without any further purification and used for the synthesis of graphene oxide. Meanwhile, titanium tetrabutoxide (TBOT) (purity: 97.0%), hydrogen fluoride ( $\text{HF}$ ) (purity: > 99%), and acetone were purchased from Sigma-Aldrich and used for the synthesis of  $\text{TiO}_2$  (001) nanoparticles. Methylene blue (MB), crystal violet (CV), and absolute ethanol were purchased from Sigma-Aldrich and used in photocatalytic degradation.

### **3.3. Synthesis of Graphene Oxide**

GO was synthesized through a modified Hummer method. The synthesis of GO was conducted through a modified Hummer method (Marcano et al., 2010). Typically, 1 g of graphite flakes and 0.5 g of  $\text{NaNO}_3$  were mixed in 25 mL of  $\text{H}_2\text{SO}_4$  and stirred for 30 minutes in an ice bath (0 °C). 3 g of  $\text{KMnO}_4$  was constantly added while keeping the temperature below 20°C for an hour. After that, the temperature was increased to room temperature and stirred for 3 hours. The mixture was then slowly diluted with 50 mL of distilled water and stirred at 90–95 °C. 100 mL of distilled water was added to the mixture,

followed by 50 mL of H<sub>2</sub>O<sub>2</sub> at 30% to stop the reaction. The resulting suspension was washed several times using HCl and distilled water until the pH was neutral. The obtained product was dried at 60 °C for 12 hours to produce dark brown GO powder.

#### **3.4. Synthesis of TiO<sub>2</sub> nanosheets with (001) facet exposure**

The synthesis of TiO<sub>2</sub> (001) exposure was carried out using the solvothermal method. Initially, 1.5 mL of HF was added to 5 mL of TBOT dropwise, followed by stirring with a magnetic stirrer. The mixture was transferred into a 200-mL Teflon-lined autoclave while keeping the temperature at 180 °C for 24 hours. After the reaction, the mixture was cooled to room temperature, and the resulting supernatant and precipitate were separated by centrifugation. The residue was washed with distilled water and ethanol several times and dried at 70 °C for 6 hours.

#### **3.5. Synthesis of Graphene Oxide/TiO<sub>2</sub> Nanocomposite**

In this study, 0.5 g of as-prepared GO was dispersed in a mixture of ethanol and water with a ratio of 1:2 (v/v) using the ultrasonic treatment for an hour to exfoliate the GO entirely. The mixture was stirred for two hours to obtain a grey suspension. The suspension was placed in a Teflon-sealed autoclave and maintained at 120 °C for 5 hours. After the reaction was complete, the product was cooled to room temperature. The precipitate was then filtered and washed using distilled water and ethanol, and it was dried at 60 °C for 15 hours to obtain nanocomposite.

### **3.6. Characterization**

Various characterizations were conducted to evaluate photocatalysts' physical and chemical properties. X-ray diffraction (XRD) analysis was carried out to determine the crystalline structure of the sample using the AERIS Benchtop X-Ray Diffractometer Malvern Panalytical with Cu-K radiation as the source radiation. Fourier-transformed infrared (FTIR) (Shimadzu IRPrestige-21) determined the functional groups of the sample by using Fourier-transformed infrared (FTIR) (Shimadzu IRPrestige-21). In addition, Raman spectroscopy was also conducted to determine the characteristic band of the as-prepared photocatalyst by using HORIBA iHR320. Finally, the morphology of the photocatalysts was analyzed with the TECNAI G2 Spirit Twin High-Resolution Transmission Electron Microscope (HR-TEM).

### **3.7. Photocatalytic Activity Studies**

The photodegradation of dyes was used to study the photocatalytic activity of the samples. This research used methylene blue, rhodamine b, crystal violet, and a mixture of the three dyes to represent the persistent organic pollutant. A 12-watt LED strip lamp (Phillip) was a visible light source. 50 mg of photocatalyst was added to 50 mL of a 10 ppm dye solution. The suspension was stirred in the dark for 10 minutes to achieve adsorption-desorption equilibrium. The visible light source (LED strip lamp) was tied to the beaker glass until it covered the entire glass surface. After the solution was stirred without a lamp, it was placed into the glass covered with an LED lamp. Under visible light exposure, 4 mL of sample suspension was mixed and taken out every 2 minutes. It repeated 5 times until the time reached 10 minutes. Each of the dye solution samples went through the same method of degradation. After degradation, ultrasonic was used to separate the photocatalyst

from the solution and to suspend it on the bottom of the glass. The remaining degraded dye solution was then measured by UV-visible spectroscopy to determine the halting waste in the mixture.

### **3.8. Analysis for measuring the dye concentration, degradation, and removal percentage**

The removal percentage was analyzed after measuring the dye concentration with UV-visible spectroscopy. For the calculation of an analytic concentration from the absorbance data obtained from the UV-visible spectroscopy, the Lambert-Beer Law (Equation 7) can be used as follows :

$$\text{Absorbance } (A) = C \times \lambda \times \varepsilon \quad (7)$$

Where C is the concentration of the dyes,  $\lambda$  is the wavelength, and  $\varepsilon$  is the extinction coefficient.

The concentration of the initial solution and concentration after photodegradation were then used to calculate the removal percentage and degradation efficiency. The degradation efficiency of the photocatalyst towards the dye solution was determined as follows (Equation 8):

$$\text{Photodegradation efficiency } (\%) = \frac{C_0 - C_t}{C_0} \times 100\% \quad (8)$$

$C_0$  and  $C_t$  (mg/L) are dyed' initial and equilibrium concentrations in an aqueous solution. 80% - 90% or more degradation efficiency is considered outstanding or highly efficient photodegradation (H. Liu et al., 2018).

### 3.9. Kinetic Studies

In this study, the kinetics of photocatalytic degradation of MB, RhB and CV using the as-prepared GO, TiO<sub>2</sub> (001), and nanocomposites were estimated using the Langmuir-Hinshelwood kinetics model, as given in the following (Equation 9):

$$\ln \frac{C_0}{C_t} = K_{app} t \quad (9)$$

The kinetic rate constant,  $K_{app}$  ( $\text{min}^{-1}$ ), was calculated from the slope of  $\ln \frac{C_0}{C_t}$  Vs. irradiation time. The reaction rate, adsorption step, surface reaction steps, and rate constant of the reaction could be determined by kinetic studies.

## CHAPTER 4: RESULT AND DISCUSSION

### 4.1. Synthesis of Graphene Oxide

This research synthesized graphene oxide using the modified Hummer method from graphite flakes. The main point of the Hummer method is the role of sulfuric acid as the solvent. Potassium permanganate and sodium nitrate were used as oxidants. The Hummers method is a simple and fast method to synthesize graphene oxide. However, this method had several drawbacks, such as the formation of toxic gases ( $\text{NO}_2$ ,  $\text{N}_2\text{O}_4$ , and  $\text{ClO}_2$ ) that can be explosives and incomplete oxidation results. A few alterations have been made with different strategies.

With the corresponding adjustment, graphene oxide was made using the following process: The temperature was kept at  $0\text{ }^\circ\text{C}$  to prevent overheating and explosions while adding other materials. The transformation from graphite to graphene oxide through the Hummer method initiates the oxidation process facilitated by potassium permanganate's action on graphite. The oxidation occurs between the graphene and sulfuric acid as the solvent. Sulfuric acid significantly impacted the intercalation process from graphite flakes to graphene oxide. Intercalation is the process by which ions or molecules appear between the layered materials.

Potassium permanganate is the oxidizing agent, and sodium nitrate is the catalyst, which also plays a vital role in this synthesis. The solution turned black after graphite and sodium nitrate were added. Kalium permanganate was added carefully by keeping the temperature below  $20^\circ\text{C}$ . Potassium permanganate reacts to form manganese heptoxide ( $\text{Mn}_2\text{O}_7$ ).  $\text{Mn}_2\text{O}_7$  is an active compound in graphene oxidation. Other species, like the permanganate ion,

may also contain excess and play a role in the reaction. The oxidant compounds have access to fill the space in the graphene layers.

Several functional groups, such as hydroxyl (-OH), epoxide (-O-), and carboxylic acid (-COOH), react with the graphene and form graphene oxide. The reaction is then extinguished by water and hydrogen peroxide to stop the oxidation reaction. The water addition formed  $\text{HMnO}_4$  by reacting with potassium heptoxide. Purification was completed by removing impurity ions from unoxidized or under-oxidized graphite. Graphite oxide must also be exfoliated to form single-layer graphene oxide through mechanical, sonication, stirring, and thermal processes. The synthesized graphene oxide manifested as a dark complexion with a slightly coarse texture. Its distinct black appearance and slight irregularity in surface morphology were discernible upon observation, underscoring its potential for photocatalytic degradation material.

#### **4.2. Synthesis of $\text{TiO}_2$ (001) exposure using a solvothermal method**

The formation of nanoparticles is a crucial element within the realm of new materials for photocatalytic degradation. Numerous methods have been devised to procure specific nanomaterials, allowing for precise control over their shape, size, dimensions, and structure. This control enables the exploration of new physical properties and unlocks innovative applications across various fields. The solvothermal method used throughout this exploration offers a versatile and efficient approach for synthesizing  $\text{TiO}_2$  nanoparticles with controlled crystal facet exposure, making it a suitable choice for this research to explore the unique properties of  $\text{TiO}_2$  (001) exposed nanomaterials as a new type of dye degradation material.

This study relies on TBOT (Titanium (IV) Butoxide) as the primary precursor for synthesizing nanocrystals. TBOT, an alkoxide derived from titanium sources, is pivotal in initiating the synthetic pathway. In the TBOT molecule, oxygen atoms covalently bond the titanium atom to the four butoxide groups. The butoxide groups act as ligands, forming coordination bonds with the titanium atom (Figure 4.1). Alkoxides, recognized for their versatility, are the critical reactants in generating diverse metallic and non-metallic compounds due to their facile reaction with water. As a precursor, TBOT undergoes chemical transformations preceding the formation of the desired compound during the synthesis process. Active utilization of TBOT underscores its significance in synthesizing nanocrystals, emphasizing its pivotal role in facilitating the reaction pathway toward desired product formation.

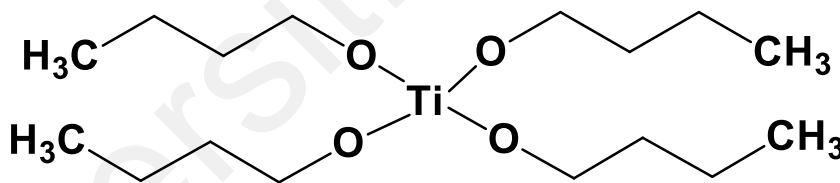
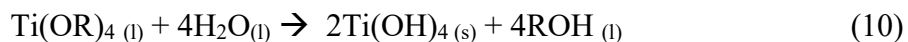


**Figure 4. 1: TBOT Chemical Structure**

Anatase  $\text{TiO}_2$  crystals are created through hydrolysis reactions starting with TBOT, which is hydrolyzed as a precursor to titania. The hydrolysis of TBOT is an essential step in the transformation process, where adding water triggers the rupture of chemical bonds within the precursor molecule. It has been documented that various techniques exist for generating  $\text{TiO}_2$  nanoparticles involving crystal nucleation and growth within Ti (IV) solutions maintained at low temperatures. Active exploration of these methods highlights their efficacy in facilitating the production of  $\text{TiO}_2$  nanoparticles with controlled



characteristics, thus underscoring their relevance in nanomaterial synthesis. The hydrolysis reaction in the water is shown in Equation (10).



In this reaction, the solvent is the most prominent component supporting hydrolysis. Many researchers have reported that the configuration of the crystal is widely influenced by the solvent, impurities, and preservative materials in the solution. It is caused by the fact that each of the different solvents has a distinct surface atomic array and surface affinity. Additionally, other solvents can modify growth rates and the final shapes of the materials (Ong et al., 2014). The role of solvents and additives in controlling the final form of the nanomaterials is illustrated in Figure 4.2. In order to achieve enhanced reactivity, the alkoxide underwent dissolution in alcohol prior to its combination with water. Ethylene glycol served as the solvent for producing the TiO<sub>2</sub> (001) nanocrystals.

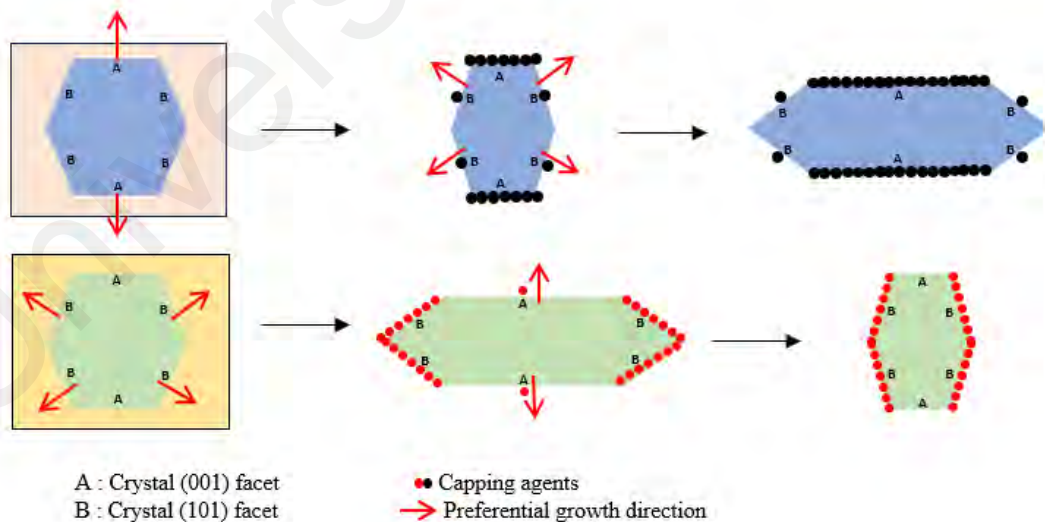


**Figure 4. 2: The schematic role illustration of solvent and additives on the morphology control of crystal (001) and (101) facets.**

Many methods have been developed to determine the TiO<sub>2</sub> (001) pathways. Surface fluorination is the most suitable and excellent method to keep the (001) exposure in TiO<sub>2</sub> anatase nanocrystals (Ong et al., 2014). The superficies analysis and mathematical calculation results explain that fluorine atoms are approvingly able to be absorbed on the 001 facets. The bond between fluorine and TiO<sub>2</sub> can lead to lower surface energy, resulting in excellent stabilization of the (001) facets of TiO<sub>2</sub> nanocrystals. Hydrofluoric acid (HF) was used as a capping agent (Sajan et al., 2016). Capping agents' role is also crucial to reducing nanomaterials' free energy because of their surface adsorption ability. It is also notable for its adsorption selectivity.

Through the hydrolysis of TBOT, TiO<sub>2</sub> crystals develop progressively during the solvothermal process. Ti-O-Ti takes less time to develop, which is superior at producing anatase single crystals thanks to the maintained hydrolysis rate aided by HF.

TiO<sub>2</sub> (001) crystals are anticipated to form at the 200 °C temperature utilized for solvothermal synthesis. The formation of TiO<sub>2</sub> (001) crystals does not require high temperatures. Anatase will convert structurally into rutile if the synthesis temperature is too high. Because anatase TiO<sub>2</sub> has a larger surface area than rutile and brookite crystals, it has a greater capacity for photocatalysis.

To create high-quality TiO<sub>2</sub> (001) nanoparticles, TiO<sub>2</sub> was synthesized using an autoclave, keeping temperature and pressure constant. The nucleation, growth mechanisms of the particles, and response rate govern the size and shape of TiO<sub>2</sub> particles. Precipitate and supernatant are produced via an autoclave-based solvothermal process. Approximately 0.5 to 0.7 g of TiO<sub>2</sub> (001) is produced per synthesis as the final result. The titanium dioxide

(TiO<sub>2</sub>) nanocrystal synthesized via solvothermal methods exhibits a powdery morphology with a refined structure and a whitish-grey colour.

Combining semiconductor and carbon-based materials is one of the best ways to overcome the drawbacks of semiconductor photocatalysts. It is one of the most promising methods because of its ability to cover a large wavelength of visible light and reduce electron-hole recombination. In this research, the synthesis of TiO<sub>2</sub>/GO nanocomposites is conducted using the solvothermal method.

Initially, graphene oxide was dissolved in the water-ethanol mixture (Figure 4.3). The solution was dispersed using the ultrasonic cleaner for an hour. The ultrasonic path was chosen to achieve maximum graphene oxide shell exfoliation. Graphene oxide (GO) possesses hydrophilic characteristics. Graphene oxide (GO) is made up of graphene sheets with carboxylic groups (COOH) on the edges, epoxide groups (-C-O-C), and hydroxyl groups (-OH) on the base plane. Electrostatic repulsion between the sheets can come from the ionization of the COOH edge group. This method enables the sheet to create water-borne suspended dispersions.

The solvents employed are ethanol and water, a dispersion and stability solvent. The polarity of ethanol significantly influences the selection of solvent. The mixture of graphene oxide can be easily dissolved in ethanol. In addition to ethanol, water is used as a solvent. A solution of ethanol and water will ideally exfoliate graphite oxide into graphene oxide. The graphene oxide is uniformly dispersed in the solvent combination to produce a stable suspension.

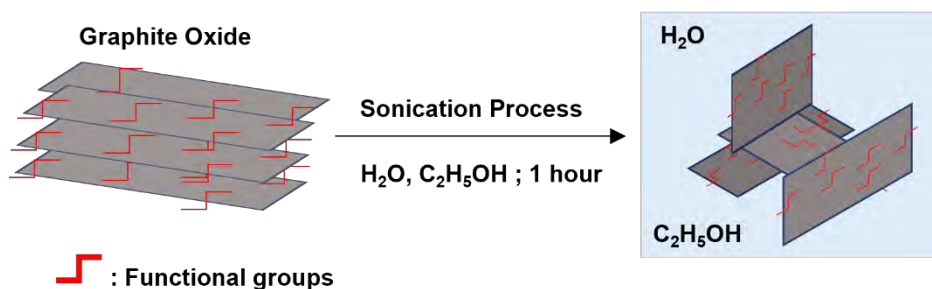


**Figure 4. 3: Fabrication of colloidal solution of exfoliated graphene nanosheets in water: ethanol solution using ultrasonic technology**

After the graphene oxide had dissolved in the ethanol and water mixture,  $\text{TiO}_2$  was added to the dispersion and then treated with ultrasonics for 60 minutes. An ultrasonic method was carried out to obtain optimal interaction between the surface of graphene oxide,  $\text{TiO}_2$ , and the solvent. This research used a solvothermal method to synthesize  $\text{TiO}_2$  and GO nanocomposites. It is necessary to keep the system temperature and pressure constant during the synthesis process, which takes place in an autoclave, to produce nanocomposites with optimal properties. The process produces supernatant and precipitate, which are rewashed with water and ethanol. Water and ethanol used for washing are added to remove impurities that can inhibit the activity of the nanocomposite. The resulting material is then filtered with a Buchner filter to remove excess solvent. Finally, the nanocrystals were dried in an oven for 24 hours.

Synthesizing nanomaterials using the solvothermal method changes the colour of the resulting nanocomposite. Graphene oxide, which is dark brown, is reacted with  $\text{TiO}_2$  P25, a white powder, with an ultrasonic process and heating and drying at  $80\text{ }^\circ\text{C}$ , resulting in a faded grey  $\text{TiO}_2/\text{GO}$  nanocomposite. The nanocomposite exhibits a powdery texture characterized by a lack of smoothness yet devoid of roughness.

The crystal structure and phase of the as-prepared samples, which were TiO<sub>2</sub> P25, TiO<sub>2</sub> (001), GO, TiO<sub>2</sub> P25/GO, and TiO<sub>2</sub> (001)/GO nanocomposite, were identified using XRD analysis, as shown in Figure 4.4 (a). The XRD spectrum displays peak variation based on the crystal properties of the nanomaterials. Atomic arrangements can also be obtained through XRD spectra analysis. The atomic arrangement for solid materials consists of crystalline and amorphous. Crystal molecules are arranged repeatedly and regularly within a long chemical chain. On the other hand, amorphous materials are composed of an irregular particle structure and have an unstable arrangement, either chemically or physically (C. Guo et al., 2021). The GO spectra exhibit an amorphous diffraction pattern with a wide, broad diffraction peak around 15°. The peaks certainly aim at the (001) plane, which describes the arrangement of graphite oxide through the oxidation process and the existence of oxygenated functional groups to develop GO nanoparticles (Yunarti et al., 2022). Furthermore, indicating the diffraction spectra at 24.5° is decent as crystal plane (002). The plane shows a partial uncompleted reaction between the oxygenated functional groups and the carbon layer to create GO. TiO<sub>2</sub> P25 and TiO<sub>2</sub> (001) diffraction pattern shows that both TiO<sub>2</sub> nanoparticles could be distinguished as crystal anatases without detecting rutile and brookite phases (Sanjaya et al., 2023). These outcomes state that (001) facet exposure using HF does not affect the crystallinity of TiO<sub>2</sub> P25 anatase (Kaushal et al., 2019). The data is sustained by the Bragg's Peaks at 25.3°, 37.8°, 48°, 53.42°, 55.1°, 62.73°, 68.9°, 70°, and 74.69° and fits well with TiO<sub>2</sub> crystal anatase (space group: *I4<sub>1</sub>/amd*, JCPDS: 01-078-2486) (Yunarti et al., 2022). Anatase demonstrated greater photocatalytic activity despite having a lesser capacity to absorb light due to its larger band gap energy (3.2 eV) than rutile (3.0 eV). It occurs due to anatase's higher surface area, which makes it simpler to interact with water and has a lower electron-hole recombination rate than rutile.

Nevertheless, the spectra found at  $23^\circ$  were ascribed to the  $\text{TiOF}_2$  phase, denoted as # in **Figure 4.4 (a)**. When HF is present in significant quantities, the phenomenon is brought on by fluorine atoms gradually replacing O atoms in the  $\text{TiO}_2$  lattice (Zhu et al., 2022). The contrast between  $\text{TiO}_2$  peaks and  $\text{TiO}_2$  (001) peaks involves, with the inclusion of HF, a reduction in the average thickness of the diffraction pattern by 10 nm without HF for the materials and 4 nm for  $\text{TiO}_2$  (001). (Xu et al., 2021). In addition, it influences the average span of the peaks. Before the reaction with HF,  $\text{TiO}_2$  peaks exhibit an average length of 8 nm, whereas, after this reaction, the average span of the spectra extends beyond 4 times, measuring 28 nm. These results elucidate a negligible disparity between  $\text{TiO}_2$  and  $\text{TiO}_2$  (001) diffraction peaks, with the primary impact observed in the dimensions of the spectra, including their length and thickness. Additionally, the spectra of  $\text{TiO}_2$  P25/GO and  $\text{TiO}_2$  (001)/GO nanocomposite exhibit that almost all the peaks are similar to the diffraction of  $\text{TiO}_2$  P25 and  $\text{TiO}_2$  (001). As stated by the XRD data, the resemblance of these spectrum patterns verifies that the presence of GO after the nanocomposite does not affect the structure and chemical bonding of  $\text{TiO}_2$ .

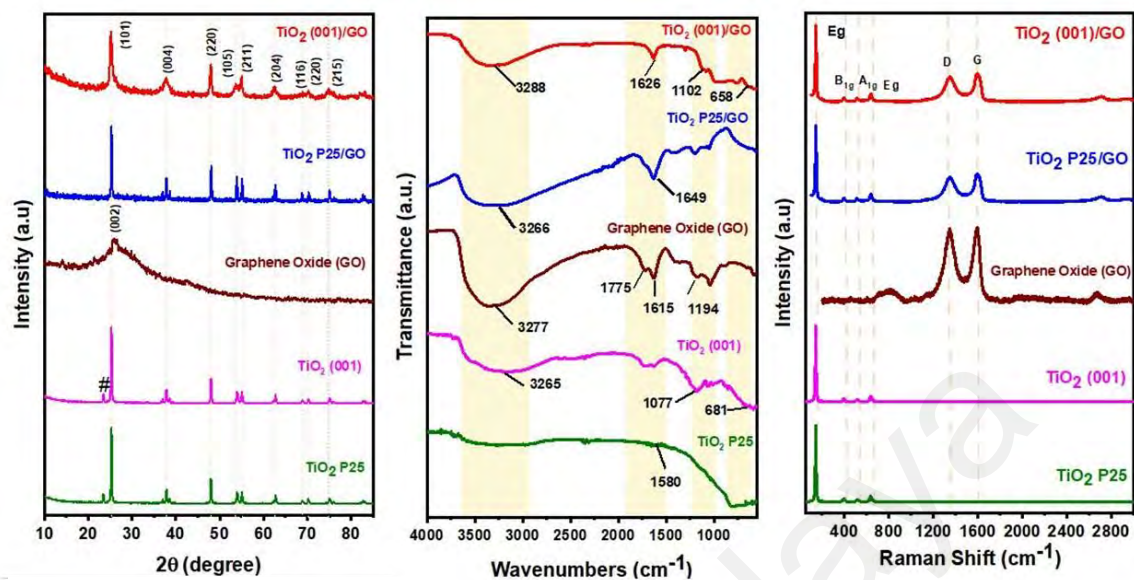


**Figure 4. 4: (a) XRD pattern, (b) FTIR spectra, and (c) Raman spectra of TiO<sub>2</sub> P25, TiO<sub>2</sub> (001), GO, TiO<sub>2</sub> P25/GO, and TiO<sub>2</sub> (001)/GO nanocomposites.**

The photocatalyst was also characterized using FTIR spectroscopy, which analyzed functional groups in TiO<sub>2</sub> P25, TiO<sub>2</sub> (001), GO, and nanocomposite, as shown in Figure 4.4 (b). The FTIR spectra of GO show the peaks indicating the C-O-C stretching vibrations at 1174 cm<sup>-1</sup> (Wang et al., 2012). In addition, double bond groups such as C=C and C=O stretching vibrations also existed at 1633 and 1720 cm<sup>-1</sup>, respectively. The IR absorption band at 1363 cm<sup>-1</sup> can also be found in the GO spectrum, attributed to the carboxyl (C-OH) bending vibration. Due to the existence of the carboxyl (COOH) group, which is known to be on GO, the broad peak at 3353 cm<sup>-1</sup> also shows the stretching vibration of hydroxyl (-OH) (Costinas et al., 2022). Considering the outcome of FTIR characterization, the availability of several oxygenated functional groups after graphite oxidation signifies that the formation of GO structures involves the intercalation of oxygen molecules at the carbon layers (Lu et al., 2013).

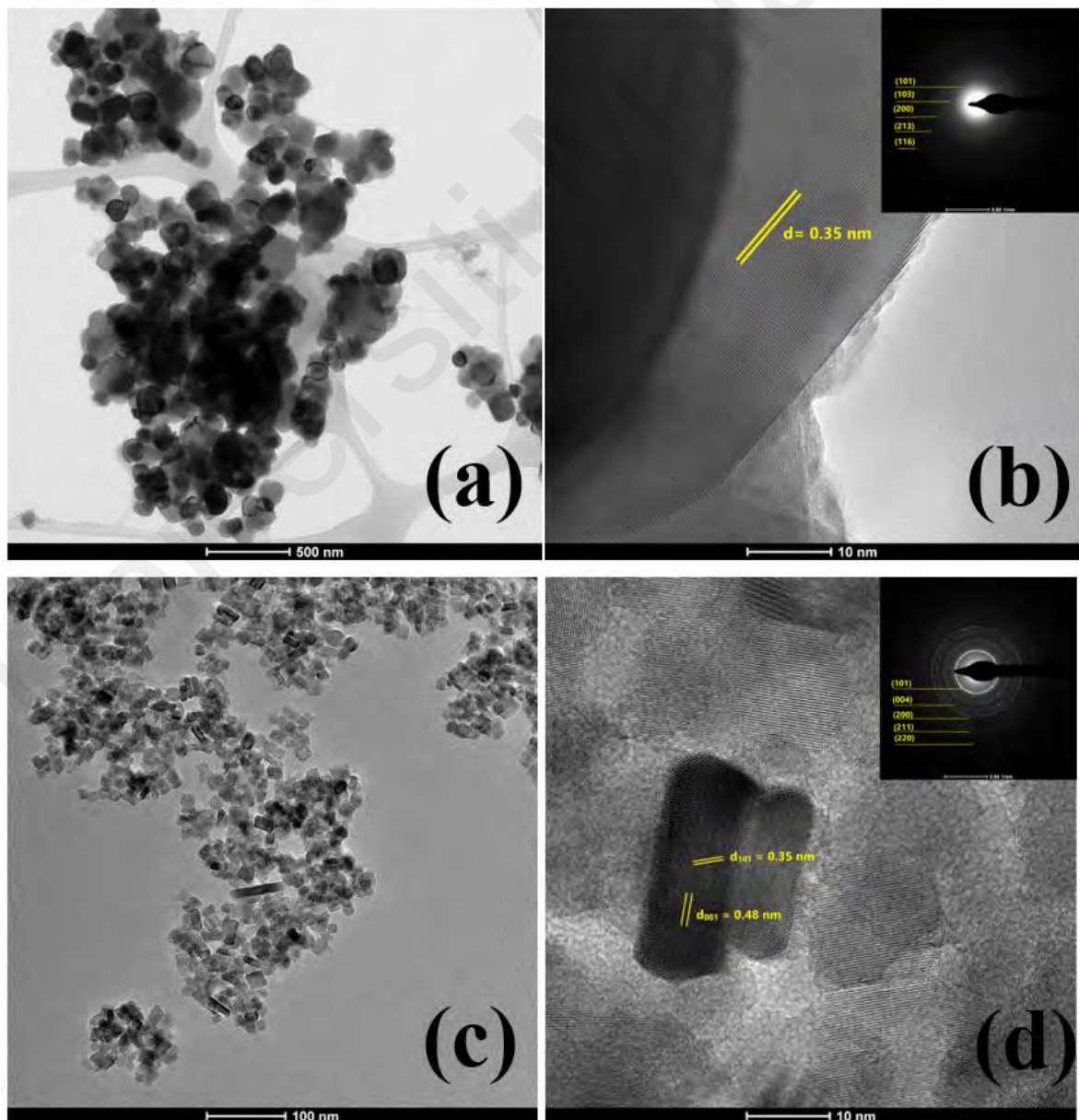
Furthermore, the oxygen-containing functional groups also play an essential role as an active site for the adsorption of TiO<sub>2</sub> on the graphene oxide. Based on the results, the FTIR spectra for TiO<sub>2</sub> P25 and TiO<sub>2</sub> (001) do not show significant differences except for the higher intensity on the TiO<sub>2</sub> (001) spectra. It denotes that the HF exposure does not cause any changes to the functional groups of TiO<sub>2</sub>. The FTIR spectra of TiO<sub>2</sub> P25 and (001) reveal that the bending vibration of Ti-O-Ti (metal, oxygen, metal) is responsible for peaks at wavenumber 580 cm<sup>-1</sup> (Qianqian et al., 2011). After the nanocomposites, the TiO<sub>2</sub> P25/GO and TiO<sub>2</sub> (001)/GO display peaks at 3200–3300 and 1610–1650 attributed to the hydroxyl groups and C=C stretching, respectively. Only TiO<sub>2</sub> (001)/GO shows the FTIR peaks at 1633 and 562 cm<sup>-1</sup>, indicating Ti-O-Ti or Ti-O-C, respectively. The phenomenon probably happened because using TBOT as the titania source made the Ti on the sample stand out even more. These vibration bands also indicate that TiO<sub>2</sub> and GO were successfully integrated to form a nanocomposite.

Figure 4.4 (c) shows the Raman analysis of the photocatalyst. A G-band peak was observed in the spectra of GO. The peak indicates the presence of in-plane vibrations of the sp<sup>2</sup> carbon atom (Muzyka et al., 2018). In addition, a D-band peak was also found at 1347 cm<sup>-1</sup>, which correlates with defects or irregularities in the sp<sup>3</sup> carbon. Consistent with the XRD and FTIR analyses, the Raman analysis of TiO<sub>2</sub> P25 and TiO<sub>2</sub> (001) also does not exhibit a considerable distinction, which explains that the exposure modification does not affect the chemical bonding intermolecular bonds. Following the Raman data, both TiO<sub>2</sub> samples exhibit a typical optical mode, such as the E<sub>g</sub> mode (142 and 637 cm<sup>-1</sup>), indicating O-Ti-O symmetric stretching vibrations on TiO<sub>2</sub>.

Moreover, O-Ti-O's symmetrical and asymmetric bending vibrations were indicated by the presence of B<sub>1g</sub> (396 cm<sup>-1</sup>) and A<sub>1g</sub> (515 cm<sup>-1</sup>) modes, respectively (Lee et al., 2018).



These results show a particular anatase  $\text{TiO}_2$  phase and confirm the XRD results. Furthermore, optical modes ( $E_g$ ,  $B_{1g}$ , and  $A_{1g}$ ), G, and D bands were visible in the Raman spectra of  $\text{TiO}_2$  P<sub>25</sub>/GO and  $\text{TiO}_2$  (001)/GO nanocomposite. These findings show that GO and  $\text{TiO}_2$  have been combined to generate a nanocomposite. The  $I_D/I_G$  ratio value between the GO and nanocomposite also varied, decreasing slightly from 0.985 to 0.88. The decreased D and G band ratio value indicates the formation of the nanocomposite. The anatase  $\text{TiO}_2$  crystal phase's formation is also linked to the decreased average size of the  $sp^2$  domain of carbon atoms (Najafi et al., 2017).



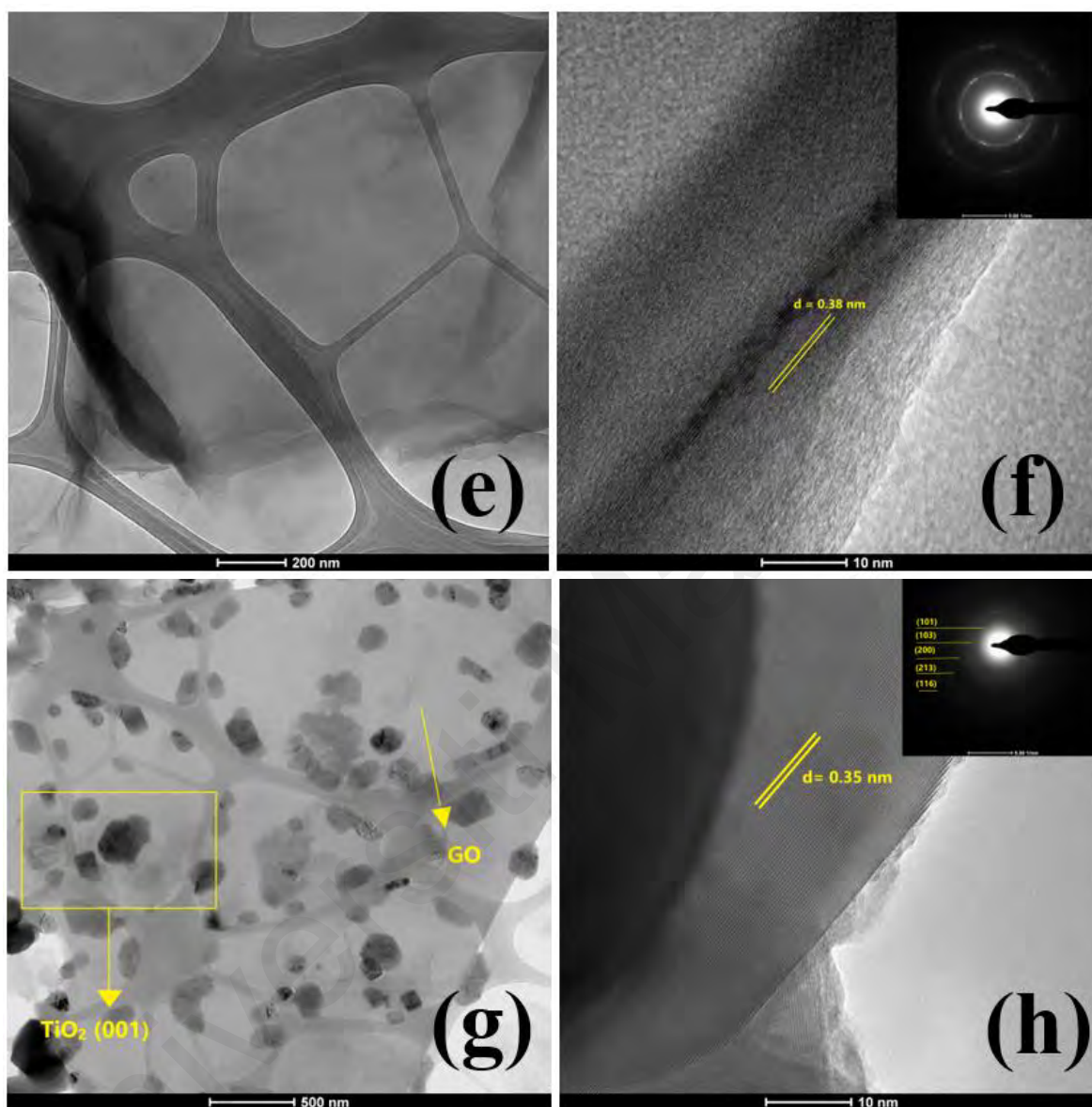


**Figure 4. 5: TEM and HR-TEM image (inset: SAED) of (a,b) TiO<sub>2</sub> P<sub>25</sub>, (c,d) TiO<sub>2</sub> (001), (e,f) GO, and (g,h) TiO<sub>2</sub> (001)/GO nanocomposite**

The morphology of the photocatalyst was determined through further investigation utilizing TEM spectroscopy. Based on the TEM data in Figure 4.5 (a), the TiO<sub>2</sub> P<sub>25</sub> nanoparticles comprise aligned nanorods and irregular particles. The irregular shape is predicted at an average of 18 nm. HRTEM images (Figure 4.5 (b)) show the lattice image

with a lattice spacing of 0.35 nm that corresponds to the (101) crystal anatase phase. The corresponding SAED pattern, shown in Figure 4.5 (b) **inset**, indicated that the material has a polycrystalline anatase structure concurrent with the XRD spectra of TiO<sub>2</sub> P25 (Dai et al., 2010).

In the bargain, Figure 4.5 (c) demonstrates the synthetic anatase TiO<sub>2</sub> (001), which is well-faceted and has a truncated tetragonal bipyramidal structure. The formation of a truncated octahedral bipyramid on TiO<sub>2</sub> (001) is due to the presence of HF in the synthesis process. HF is essential as a morphology-controlling agent in forming truncated octahedral bipyramids. In synthesis using the solvothermal method, HF also acts as a capping agent, significantly influencing the formation of facets (001). The capping agent stabilizes the (001) facets in the anatase crystals. Truncated octahedral bipyramid is the most popular crystalline form of TiO<sub>2</sub> observed in nature. It consists of eight (101) surfaces located on a side and two (001) facets on the top and bottom cut facets (Figure 4.6). During the crystal growth process under equilibrium conditions, the high-energy (001) facet decreases rapidly, causing the crystal to change to a specific shape with open facets spontaneously (Ong et al., 2014). The (001) facet is a high-energy facet, so it tends to be challenging to form, while facets (101) have relatively low energies, which causes facets (101) to form more easily.

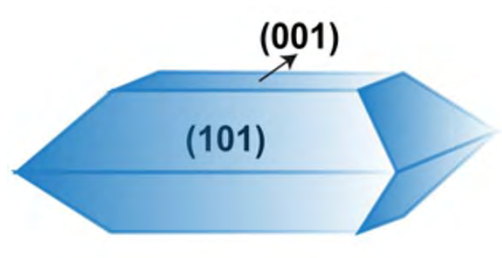


**Figure 4. 6: Truncated Tetragonal Bypiramid Structure of TiO<sub>2</sub>**

Furthermore, the unique lattice fringes of the anatase crystal phase, measured at 0.35 nm for (101) and 0.48 nm for (001), were also visible in the as-prepared TiO<sub>2</sub> (Figure 4.5(d)). This result is also confirmed by the SAED analysis (inset Figure 4.5 (d)), whose appearance is similar to the literature and the results of XRD (Loryuenyong et al., 2013; Shen et al., 2015).

Following the TEM image data (Figure 4.5 (e)), the synthesized GO has a wrinkled and fold-on sheet structure. The findings of the HRTEM (Figure 4.5 (f)) analysis provide more evidence than other characterizations in favour of the development of GO. The calculation yielded an interlayer distance of 0.38 nm. This result measures 0.335 nm larger than graphite. It also explains that the oxygen functional groups were successfully removed from multiple layers of graphite.

Before the nanocomposite, graphene oxide was typically seen as thin and relatively transparent due to oxygen-containing functional groups. The edges of GO may also appear irregular or jagged, and individual sheets may overlap or stack on top of each other. On the other hand, the TiO<sub>2</sub> before the composite would be revealed as well-defined particles with uniform size and shape. In this case, TiO<sub>2</sub> (001) has a truncated bipyramid shape. In addition, Figure 4.5 (g) displays the TiO<sub>2</sub> (001)/GO morphology after the nanocomposite was performed. It can be expected that a combination of features from both GO and TiO<sub>2</sub> will be seen. These findings demonstrated that anatase TiO<sub>2</sub> (001) was equally spread on the GO surface sheet.

Furthermore, every lattice fringe from the HR-TEM and SAED analyses (Figure 4.5 (h) and inset) shows a pattern and distinct diffraction rings that are comparable to those of TiO<sub>2</sub> (001). The TEM images may reveal modifications in the morphology and size distribution

compared to individual GO and TiO<sub>2</sub> (001) components, reflecting the formation of the nanocomposite structure. These findings support the successful formation of the TiO<sub>2</sub> (001)/GO nanocomposite.

TiO<sub>2</sub> (001) facet exposure has been successfully fabricated in this research. The lattice spacing value can discover the existence of facet (001). Raman and HR-TEM are two techniques that can be utilized to determine the percentage of (001) facets in TiO<sub>2</sub> crystal anatase. By assuming that the (001) and (101) facets fill about 100% of all surfaces, the ratio of (001) facets for the HR-TEM method can be determined (Equation 11).

$$S_{(001)} \% = \frac{\cos \theta}{\cos \theta + \left(\frac{a}{b}\right)^{-2} - 1} \quad (11)$$

Where  $S_{(001)}\%$  is the percentage of the (001) facets,  $a$  and  $b$  are the sides of (001) and (101), respectively. The value refers to the interface angle between the (001) and (101) facets of previous studies, around 68.3 (Yang et al., 2008). Using HR-TEM, the calculation reveals that 38.8% of the crystal facets (001) of TiO<sub>2</sub> are visible. This calculation is based on the number of particles visible from the TEM characterization using the ImageJ software. This study calculated the percentage of exposure to crystal facets (001) with three particles for each TiO<sub>2</sub> produced from different precursors (Yunarti et al., 2022). The approach of calculating facet exposure using HR-TEM is the materials' spatial resolution, morphology, and structure. This method is suitable for a small sample and is known as a more sensitive method since it is calculated using the angle from the TEM Images.

However, Raman spectroscopy was used to determine the proportion of exposed (001) facets, which was also quantitatively evaluated (Tian et al., 2012). The calculation using Raman spectroscopy depends on the vibration of molecular bonds between the materials.

This method also has a high sensitivity since the calculation is based on the ratio between the peak intensity of the  $E_g$  and  $A_{1g}$  peaks. Based on the Raman analysis data, the symmetric stretching vibration modes of the Ti-O-Ti bond decreased when the exposed (001) facets existed compared to the unexposed (001) crystal. The higher the (001) facet exposure percentage, the fewer the symmetric stretching vibration modes of OTiO will be. The intensity of  $E_g$  becomes less intense, consistent with the amount of stretching vibration. Contrarily,  $TiO_2$  (001) facet exposure increased Ti-O-Ti's total symmetric and antisymmetric bending vibrations. Under the higher percentage of  $TiO_2$  (001) facets, the symmetric and antisymmetric bending vibration of Ti-O-Ti will be found to lead to an increased intensity of the  $A_{1g}$  and  $B_{1g}$  peaks in the Raman spectra. According to the aforementioned theoretical analysis and experimental results, the percentage of  $TiO_2$  (001) facets exposed distinctly relates to the intensity variations of the Raman vibrational modes  $E_g$  and  $A_{1g}$ . To get the percentage of exposed 001 facets in anatase  $TiO_2$ , we suggested a different method that involved comparing the peak intensities of the  $E_g$  and  $A_{1g}$  peaks.

Hence, the percentage of  $TiO_2$  (001) facets exposed based on Raman analysis was 3.26%. This method offers excellent measurement sensitivity because the presence of bond vibrations in specific molecules results in differences in the intensity values of each vibration mode.

Both Raman and TEM analyses are appropriate for evaluating the facet exposure of  $TiO_2$  (001). The choice of method depends on the specific attributes of the material under scrutiny. TEM analysis primarily examines morphology, whereas Raman analysis primarily investigates chemical composition. The selection of the appropriate method is contingent upon sample characteristics, including size and morphology.

**Table 4. 1: TiO<sub>2</sub> (001) Facet exposure based on TEM and Raman spectroscopy analysis**

TEM Analysis	Raman Analysis
38.8 %	3.26 %

Raman and HR-TEM facet exposure calculations generate varied results, as shown in Table 4.1. Raman spectroscopy calculations are ten times out of step with the HR-TEM analysis. It can be obtained because the lattice spacing and interface angle technique identified far more exposure than the Raman spectroscopy ratio between E<sub>g</sub> and A<sub>1g</sub>. However, both (001) exposure calculation techniques demonstrate that TiO<sub>2</sub> can be effectively modified to boost photocatalytic activity using 001 exposure facets (Ong et al., 2014).

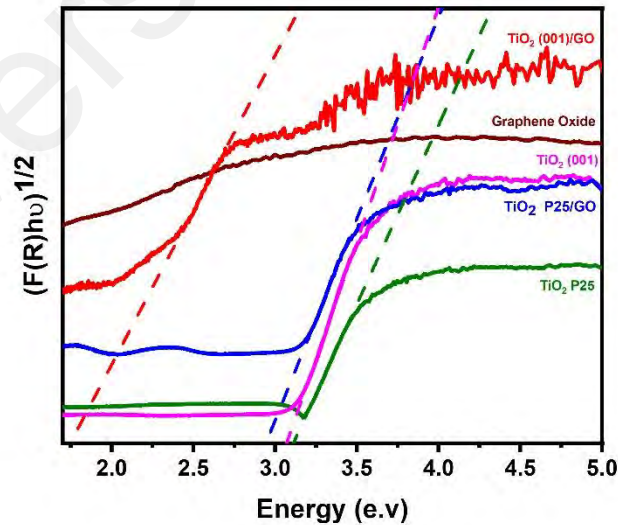


**Figure 4. 7: Kubelka-Munk plot of photocatalysts**



Optical band gap analysis was also done using UV-visible Diffuse Reflectance Spectroscopy (DRS). The wavelength and energy reflectance can be obtained from the UV-visible DRS analysis. Band gap analysis could be carried out by applying the DRS data. The band gap analysis is crucial to achieving an effective photocatalytic process. The bandgap energy of each photocatalyst synthesis can be calculated using the Kubelka-Munk equation from the known reflectance values based on the experiment mentioned above. The relation between the Kubelka-Munk value and the band gap energy is depicted in **Figure 4.7**.

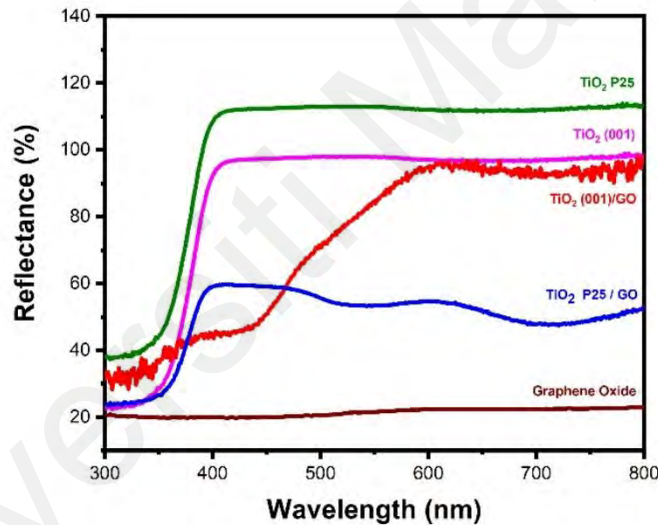


**Figure 4. 8: DRS Spectra of as-prepared photocatalyst**

The reflectance percentage obtained from UV-visible DRS measurements can be converted using the Kubelka-Munk equation to determine the bandgap energy between the conduction and valence bands. The Kubelka-Munk equation is explained in Equation (12).

$$F(R) = \frac{(1 - R)^2}{2R} \quad (12)$$



$F(R)$  is a Kubelka-Munk factor,  $K$  is the absorption coefficient, and  $S$  and  $R$  are ascribed as the scattering coefficient and reflectance value, respectively. Studying the linear area of the UV-visible DRS curve is required to determine the band-gap energy value. Plotting the  $h\nu$  (eV) on the x-axis with  $[F(R) h\nu]^{1/2}$  on the y-axis yields the curve. In addition, the DRS spectra or % reflectance of photocatalysts are also shown in Figure 4.8.

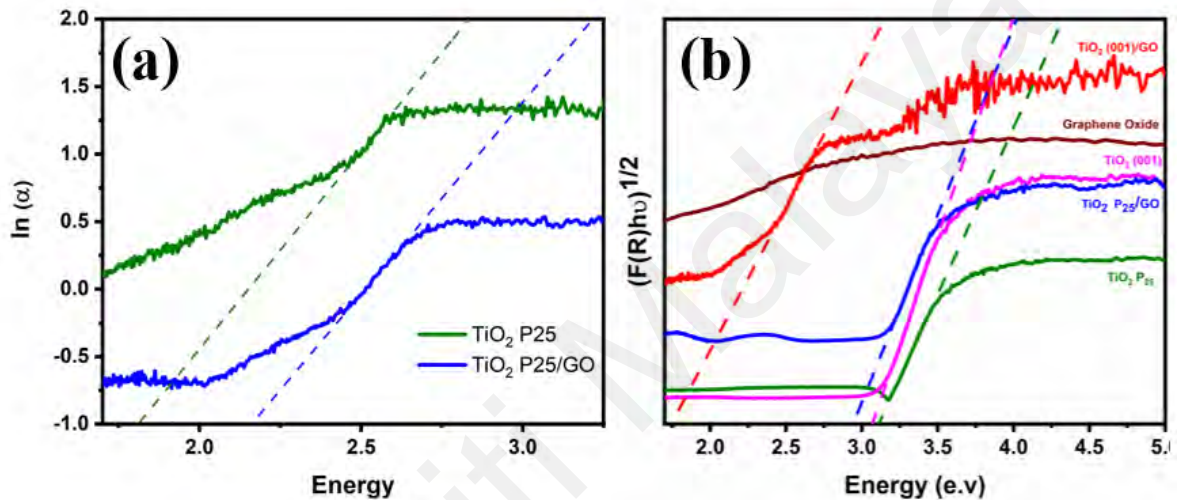


**Figure 4. 9: (a) Urbach Energy of TiO<sub>2</sub> (001) and TiO<sub>2</sub> (001)/GO, and (b) Urbach Energy of TiO<sub>2</sub> P25 and TiO<sub>2</sub> P25/GO nanocomposite.**

By employing the Kubelka-Munk equation to estimate the band gap energy, it was discovered that TiO<sub>2</sub> (001)/GO has a lower value for the band gap energy than other photocatalysts. Commercial TiO<sub>2</sub> or TiO<sub>2</sub> P25 has a band gap energy of 3.20 eV and is only photo-catalytically active when exposed to UV light. After modifying TiO<sub>2</sub> (001) exposure, the band gap shows a lower value of 3.07 eV. The decrease in band gap energy is thought to be due to the presence of (001) facets exposed to the TiO<sub>2</sub> nanocrystal.

Facet (001) occurs due to oxygen vacancy. Oxygen vacancy occurs when the amount of oxygen in certain compounds is less than it should be and leads to an imperfect crystal lattice (Adormaa et al., 2018). This oxygen vacancy affects the escalation of the

photocatalytic ability of the nanoparticles. It is applied because the Ti atom binds the O atom in a pentacoordinate manner, making it more electronegative. The binding causes the fermi level to be lower, leading to a smaller band gap energy since the electrons in the valence band become excited. Hence, TiO<sub>2</sub> (001) will be photo-catalytically active and more efficient in the visible area. Moreover, the smaller band gap caused by the oxygen vacancy can also be observed when the impurity state becomes more delocalized, overlaps the valence band edges, and increases the position of the valence band. Additionally, visible light is absorbed more effectively, according to the theory (Zhao et al., 2012).

Integrating TiO<sub>2</sub> (001) with GO causes a lower band gap energy of 2.96 eV for TiO<sub>2</sub> P25/GO and 1.74 for TiO<sub>2</sub> (001)/GO. FT-IR spectroscopy shows that this decrease in band gap energy is made possible by the increased availability of surface oxygen groups in GO, which can interact with TiO<sub>2</sub> nanoparticles to create Ti-O-C chemical bonds in the nanocomposite (Tayel et al., 2018). These results imply that GO alters the optical properties of the TiO<sub>2</sub> band gap, decreasing the energy band gap to boost photocatalytic activity and enlarging the visible-light photoactive area (Arshad et al., 2020).

Furthermore, the decrease in band gap energy is also related to the occurrence of the defect after the nanocomposite with graphene oxide. The Urbach tail, related to Urbach energy, is an absorption tail that extends deeply into the forbidden gap due to a localized fault (Khalil et al., 2020). Urbach energy can be estimated using the following equation 13:

$$\alpha = \alpha_0 \exp\left(\frac{E}{E_u}\right) \quad (13)$$

Where the absorption coefficient is explained,  $E$  refers to the photon's energy, and  $E_u$  is the corresponding Urbach energy.  $E_u$  was determined as the slope of the linear portion

reciprocated by  $\ln$  vs. photon energy ( $E$ ). The Urbach energy plot of the photocatalyst is shown in Figure 4.9 (a) for  $\text{TiO}_2$  (001) and  $\text{TiO}_2$  (001)/GO, as well as in Figure 4.9 (b) for  $\text{TiO}_2$  P25 and  $\text{TiO}_2$  P25/GO. Based on the calculations, the  $E_u$  value for nanocomposites (0.21 eV) was found to be more than five times greater than the  $\text{TiO}_2$  (001) (0.04 eV). It can also be discovered that the Urbach energy of  $\text{TiO}_2$  P25 is 0.03, while the nanocomposite reached a significant value of 0.34 eV. Per prior research by Zhong et al., the number of structural defects correlates with absorption tailing (Zhong et al., 1992). It was also reported that the rise in Urbach tailing energy was caused by the accumulation of oxygen vacancies in  $\text{TiO}_2$  due to structural instability caused by integration with CdSe nanoparticles. Similar results were obtained in earlier investigations using GO and polyvinyl alcohol (PVA) nanocomposites, which offered high Urbach energy. Interestingly, the Urbach energy value increases with GO concentration in the supplied nanocomposite, which is related to improved interaction between GO surface oxygen groups and PVA surface oxygen groups (Abu Hurayra–Lizu et al., 2021). As a result, the Urbach energy value in our case is higher than that of  $\text{TiO}_2$  (001) because the integration of GO into  $\text{TiO}_2$  (001) may lead to the formation of oxygen vacancies and structural flaws.

Moreover, the Butler-Ginley method can determine the theoretical band structure based on the predicted band gap energies. The following equations 14–15 are applied to estimate the valence band (VB) and conduction band (CB) values:

$$E_{CB} = X - E_c - 0.5E_g \quad (14)$$

$$E_{VB} = E_{CB} + E_g \quad (15)$$

Where  $X$  is the Mulliken electronegativity of  $\text{TiO}_2$  (5.9 eV),  $E_c$  expresses the energy of the free electron concerning hydrogen (4.5 eV), and  $E_g$  is the determined Kubelka-Munk band

gap energy (eV). The band gap, band structures, and Urbach energies of the nanomaterials TiO<sub>2</sub> P25, TiO<sub>2</sub> (001), TiO<sub>2</sub> P25/GO, and TiO<sub>2</sub> (001)/GO are summarized in Table 4.2.

**Table 4. 2: Band gap, band structures, and Urbach energies of the as-prepared photocatalyst.**

Photocatalyst	Band gap energy (eV) <sup>a</sup>	Valance band (eV) <sup>b</sup>	Conduction band (eV) <sup>b</sup>	Urbach energy (eV)
TiO <sub>2</sub> P25	3.12	+2.96	-0.16	0.03
TiO <sub>2</sub> (001)	3.07	+2.93	-0.13	0.04
TiO <sub>2</sub> P25/GO	2.96	+2.88	-0.08	0.35
TiO <sub>2</sub> (001)/GO	1.74	+2.27	0.53	0.21

<sup>a</sup> Kubelka-Munk equation

<sup>b</sup> Butler-Ginley approach (vs. standard hydrogen electrode (NHE))

### 4.3. Evaluation of Photocatalytic Performances

After the characterization and synthesized processes were completed, the as-prepared photocatalyst was evaluated to investigate the photocatalytic activity. This study used Methylene Blue, Rhodamine B, Crystal Violet, and a combination of these three dyes as dye modules to conduct the photocatalytic evaluation. Primarily, molar absorptivity ( $\epsilon$ ) was determined before the examination. Molar absorptivity is measured as the capacity of the catalysts to absorb light at specific wavelengths. The increment of molar absorptivity is influenced by the number of molecules going through the electron transition.

Based on the UV-visible analysis, methylene blue's lambda maximum ( $\lambda_{max}$ ) is 665 nm, while rhodamine b and crystal violet are 554 nm, respectively. The photodegradation was initially measured, followed by the measurement of the standard solution. The standard solution is required to compute the concentration of the organic dyes discovered by UV-

visible measurements. A relationship curve between the alteration in dye concentration and dye absorbance at maximum wavelength can be determined using the Lambert-Beer Law. From the curve calculation, equation 16 is obtained.

$$y = bx + c \quad (16)$$

where  $b$  is the molar absorptivity value of the dye obtained from uv-visible characterization ( $M^{-1} \text{ cm}^{-1}$ ).

The linear equation obtained from the standard diagram between the maximum methylene blue and lambda variations of methylene blue is  $y = 0.0578x - 0.0108$  with  $R^2 = 0.9998$ . From this linear equation, it can be determined that the molar absorptivity of methylene blue is  $0.00578 \text{ M}^{-1} \text{ cm}^{-1}$ . The molar absorptivity value will be used as a reference to determine the concentration of methylene blue after photodegradation.

A standard solution is also necessary using the same preparation method as the standard methylene blue solution to determine the concentration of the rhodamine B dye after photodegradation. The linear curve obtained from the Rhodamine B variation is  $y = 0.0127x + 0.0686$  with an  $R^2$  of 0.9992. The molar absorptivity of rhodamine B was also obtained at  $0.0127 \text{ M}^{-1} \text{ cm}^{-1}$ .

Following the measurement of Methylene Blue (MB) and Rhodamine B (RhB) standard solutions, Crystal Violet (CV) standard solutions are also required. Five CV standard solutions were prepared to be measured with a deep purple colour to obtain a linear curve. The  $R^2$  obtained is 0.9996, with a CV molar absorptivity of  $0.0335 \text{ M}^{-1} \text{ cm}^{-1}$ .

In addition to measuring the photocatalyst activity for the degradation of MB, RhB, and CV, this study also tested the photocatalyst activity of a mixture of the three dyes. The ratio

of the concentrations of the three dyes in the mixed solution is 1:1:1, with a concentration of 10 ppm for each solution. Measuring the standard solution, consisting of the three colouring compounds, is necessary to measure the molar absorptivity of the dye mixture solution. The linear curve obtained from the organic dye mixture is  $y = 0.0701x + 0.1168$  with an  $R^2$  of 0.9995. Furthermore, the molar absorptivity of the three dye combinations was also obtained at 0.0701.

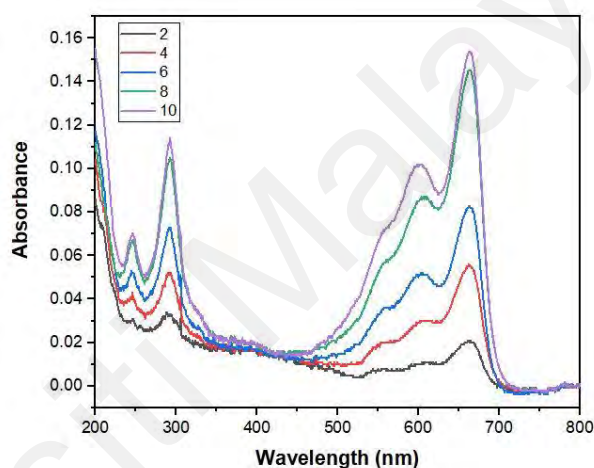
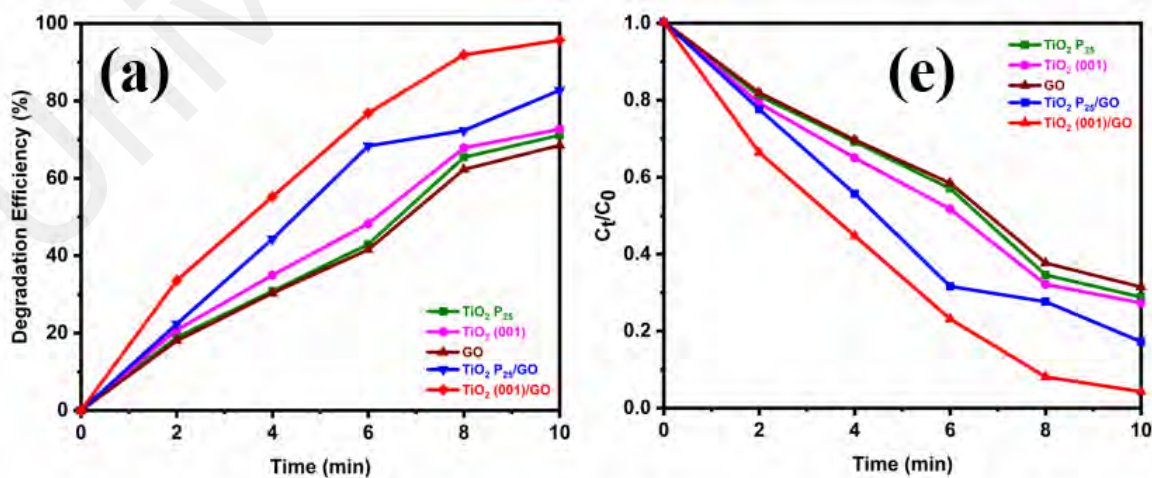


**Figure 4. 10: The absorbance spectra of dye compounds mixture**

Figure 4.10 shows that the  $\lambda_{max}$  possessed by the mixed dye solution is 657 nm. It is distinguishable that the absorbance of the mixture shifts towards an absorbance close to the  $\lambda_{max}$  of methylene blue, which is 665 nm. With the same concentration, the maximum wavelength of the dye solution mixture tends to resemble  $\lambda_{max}$  methylene blue compared to  $\lambda_{max}$  rhodamine B and crystal violet at 554 nm and 590 nm, respectively. It is expected to occur because methylene blue dyes are essential in the dye mixture. The functional groups of the organic dyes formed after mixing are expected to be similar to methylene blue.

The as-prepared catalysts are tested for their photocatalytic activity by degrading each of the three organic dyes in a mixed solution. The photodegradation test for dye solutions was carried out by mixing 0.05 grams of photocatalyst into 50 mL of the organic dyes. Then, the mixture was stirred for 2 minutes in the dark. Mixing in the dark is implemented to achieve the adsorption-desorption equilibrium of the catalyst before the irradiation process is executed by visible light.

The photodegradation process begins when the dye reacts with the photocatalyst. The dye is expected to stay outside the photocatalyst without absorbing into the nanoparticle. The absorption of dye molecules can lead to inhibition of the photocatalytic activity. The process of molecular diffusion follows adsorption. Molecular diffusion can also be referred to as a desorption process. The photocatalytic process cannot occur when the equilibrium is in the desorption process, so stirring must be carried out in the dark so that the equilibrium shifts towards adsorption. After stirring without light, the mixture was irradiated by an 11-watt LED strip lamp for 10 minutes, with removal every 2 minutes. Every 2 minutes, the MB and RB colours fade with sampling.





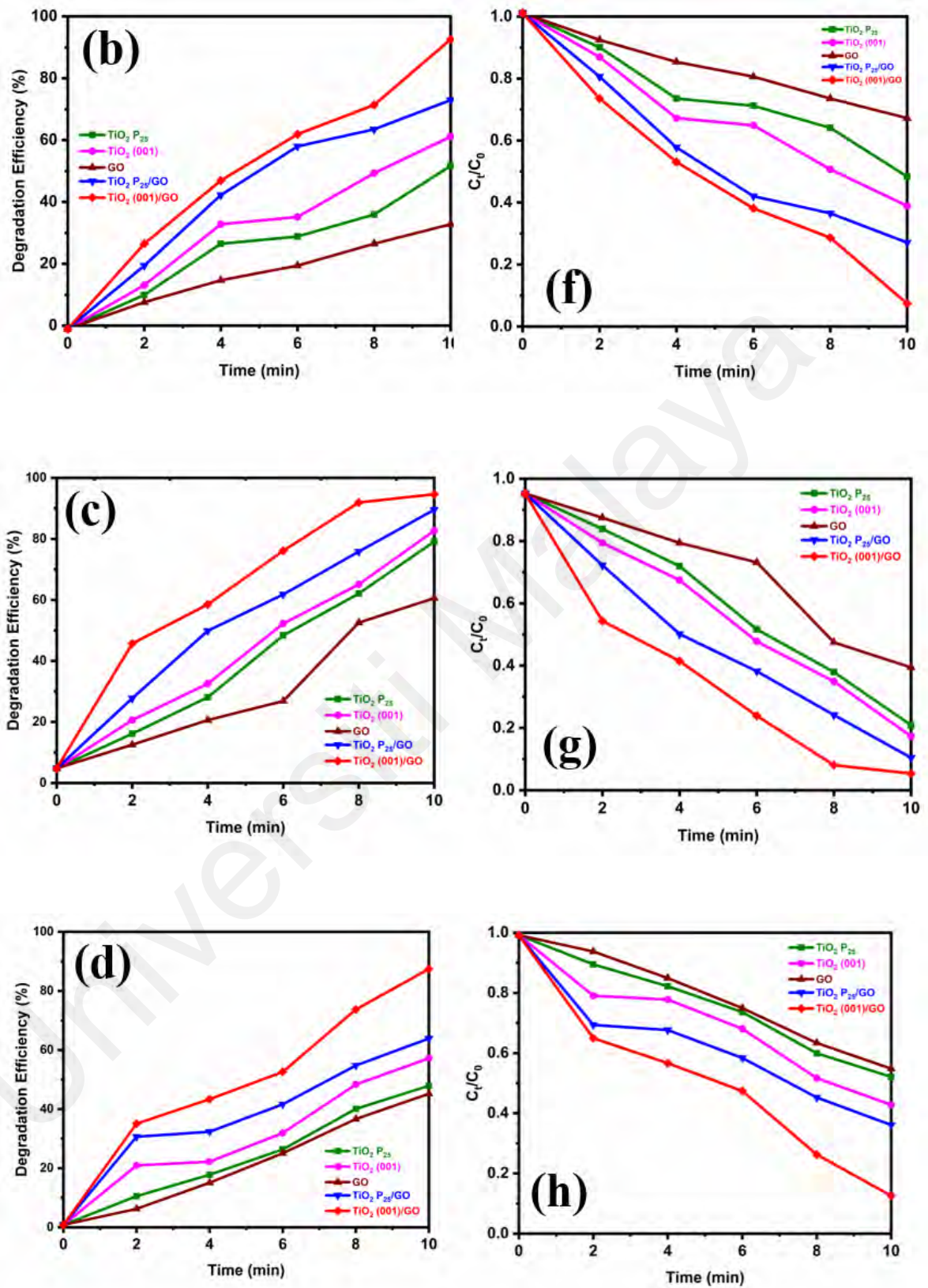


Figure 4. 11: Photodegradation efficiency and the plot of removal  $C_t/C_0$  of MB (a,e); RhB (b,f); CV (c,g); and Mix dyes (d,h)



UV-visible measurements were carried out on all samples of five types of photocatalysts to determine the concentration of organic dyes after photodegradation. As the irradiation progressed, the concentration of MB, RhB, CV, and Mix dyes in the solution rapidly dropped. The solution hue also shifted from deep blue to colourless for methylene blue. Rhodamine B samples show a colour alteration from a slight pink to a translucent solution. The CV solution also exhibits a colour change from dark purple to a very subtle purple. Lastly, the colour of mixed dyes slowly transforms from dark red to a transparent colour. The degradation rate of the dyes is calculated using the following equation (Equation 17).

$$\eta (\%) = \frac{C_0 - C_t}{C_0} \times 100 \quad (17)$$

$C_0$  is the solution's initial concentration, and  $C_t$  is the final concentration after photodegradation.

The percentage of dye degradation with the as-prepared sample was calculated and presented in Figure 4.11. In the first 10 min of the reaction, the percentage of degradation of MB, CV, RhB, and mix dyes using  $\text{TiO}_2$  (001)/GO nanocomposite was 95, 92, 94, and 87%, respectively. These results were higher when compared to GO or  $\text{TiO}_2$  (001) at the same irradiation time. Graphene oxide only exhibits 68, 32, 89, and 45% degradation efficiency for MB, CV, RhB, and mixed dyes successfully after 10 minutes of lamp irradiation. It remarks on the lowest degradation efficiency due to the characteristics of carbon materials that are more inclined to adsorb the organic dyes, resulting in the inhibition of photocatalytic activity. While  $\text{TiO}_2$  (001) shows better results at 72, 61, 60, and 57% of the photodegradation efficiency of MB, CV, RhB, and mix dyes, the degradation efficiency of nanocomposites exhibits the highest degradation efficiency.

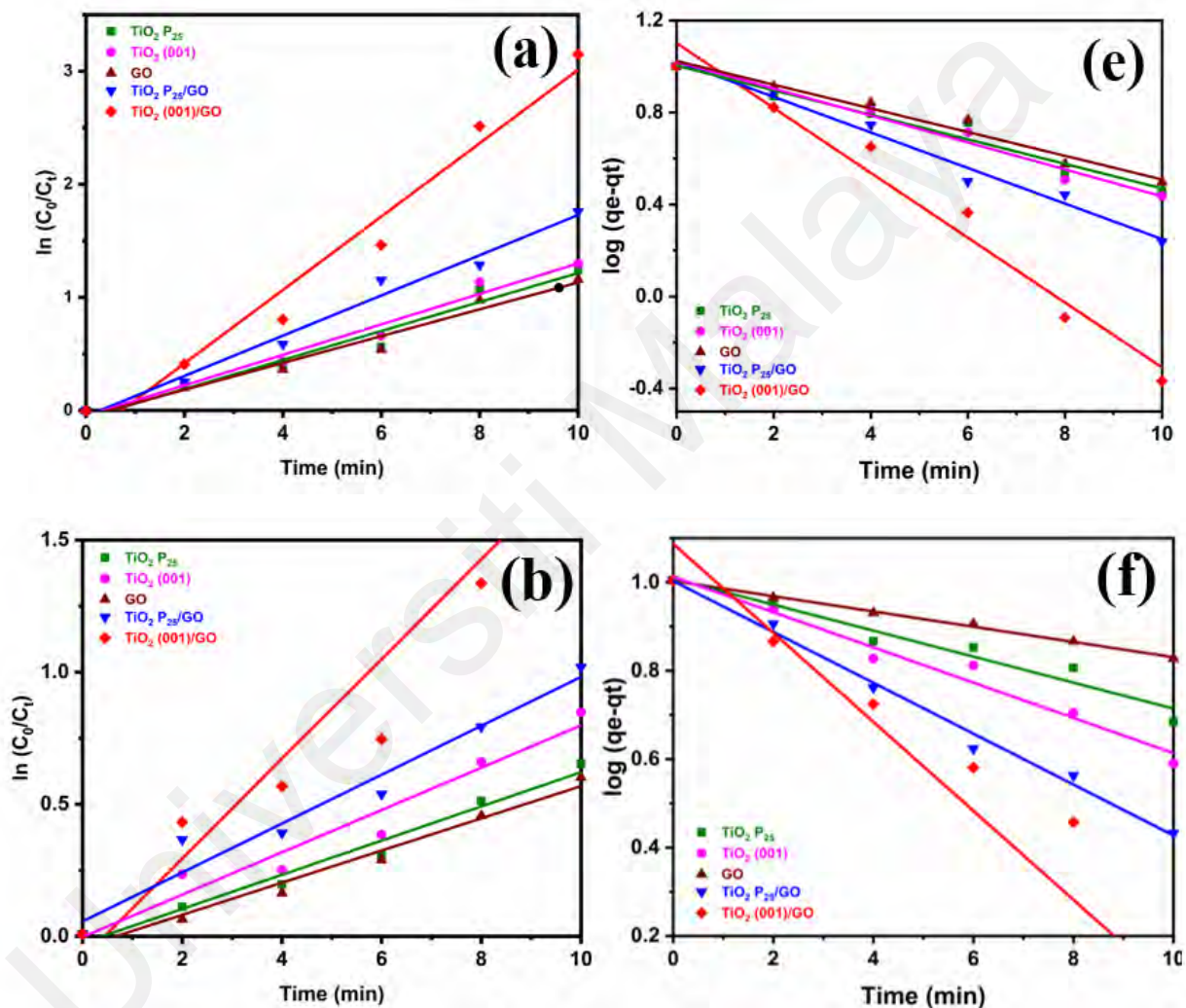
The difference in dye solutions' degradation efficiency depends on the photocatalysts' physical properties. Morphology, size, crystallinity, surface area, and band gap value play essential roles in the properties of photocatalyst nanoparticles (Khan et al., 2019). The degradation efficacy of TiO<sub>2</sub> (001)/GO nanocomposites is thought to be leading due to the rise in photocatalytic ability. The presence of facet (001) nanoparticles tends to make them more electronegative because, in this state, the Ti-O bond occurs pentacoordinate. ((Araujo-Lopez et al., 2016; Köppen & Langel, 2008). It leads to higher and more reactive surface energy for TiO<sub>2</sub> (001). Moreover, Facet (001) nanoparticles are inclined to interact with H<sub>2</sub>O, which induces radical reaction regeneration (Gao et al., 2015).

Hydroxyl radicals and superoxide radicals are the essential molecules in photocatalytic activity. In addition, band gap value degradation of TiO<sub>2</sub>/GO nanocomposite is expected to be caused by the interaction between unpaired electrons and GO on the nanocomposite surface. This case benefits photocatalytic activity due to the necessity of electrons in the reaction (Khannam et al., 2016). By integrating graphene oxide (GO) on the TiO<sub>2</sub> surface, the surface area becomes more extensive and can absorb more visible light and accept electrons.

Furthermore, increased Urbach energy supports the high photocatalytic properties of the TiO<sub>2</sub> (001)/GO nanocomposite. Due to disorder and flaws, the high Urbach energy brings about localized circumstances at or around the conduction band level. These localized states will serve as a charge carrier trapping center and aid in photocatalytic degradation. GO has the least degradation efficiency. However, because of its vast surface area and high adsorption surface for contaminating dyes, it is helpful for photocatalysis. Altering the Ti<sup>2+</sup> ion by GO in the TiO<sub>2</sub> nanostructure produces an enhanced positively charged surface. As a result, interactions between acidic and neutral environments, positively charged dye

molecules, and negatively charged catalyst surfaces promote enhanced adsorption. Thus, excellent photochemical reactivity is displayed by the TiO<sub>2</sub> (001)/GO nanocomposite when exposed to visible light.

#### 4.4. Kinetic Studies of Photocatalytic Degradation



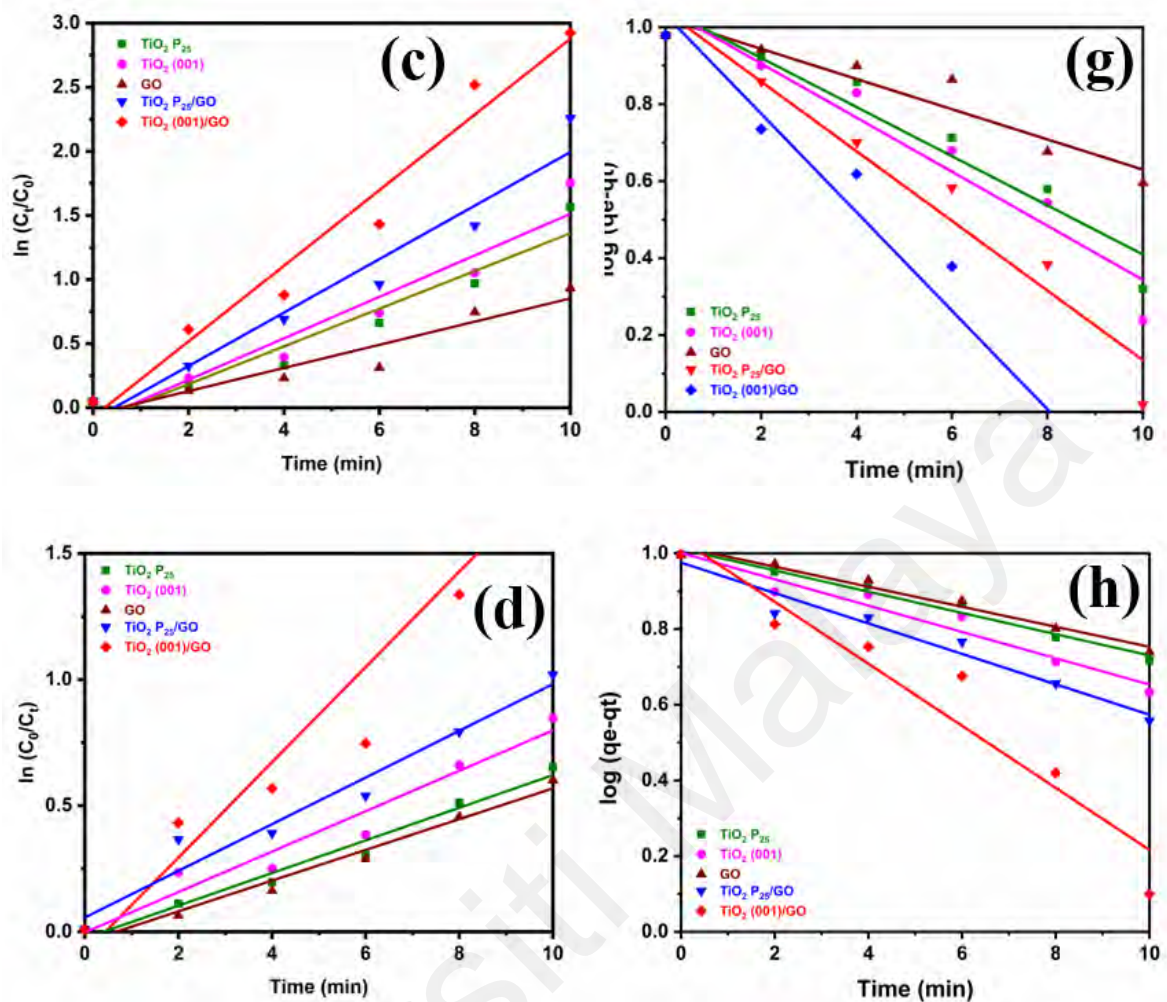


**Figure 4. 12: Pseudo-first order kinetics of (a) MB, (b) RhB, (c) CV, and (d) Mix dyes and First order kinetic of (e) MB, (f) RhB, (g) CV, and (h) Mix dyes**

The kinetic studies of photocatalytic degradation of dyes were carried out to determine the effect of the (001) facet exposure and nanocomposite on the photodegradation rate. Figure 4.12 a–d displays pseudo-first-order kinetics, while Figure 4.12 e–h shows the result of first-order kinetic degradation. The photodegradation kinetics of MB, RhB, CV, and mixed dyes follow a first-order pseudo-reaction in which an increase in the concentration of the reactants can linearly affect the photodegradation rate of the dye

solutions. At the same time, the catalyst and other conditions are kept constant so that they do not directly affect the photodegradation kinetics.

A first-order kinetic reaction is known to have a reaction rate that is linearly dependent on the concentration of a single component. In other words, a first-order reaction relies only on one of the reactants' concentration changes, resulting in a reaction rate alteration. As an outcome, the sequence of these reactions is 1. A [differential rate law](#) can describe a chemical reaction at a molecular level. On the other hand, pseudo-first-order reactions are not first-order reactions but sometimes seem to be like second-order reactions. When the concentration of one reactant is greater than the concentration of the other, the concentration of the excess reactant can be ignored. Furthermore, the whole rate of the reaction depends only on one reactant. Overall, the kinetics data ensures that the (001) exposure of TiO<sub>2</sub> and graphene oxide as a nanocomposite significantly enhances the dye photodegradation process.

#### 4.5. Possible Mechanism For Photocatalytic Performance

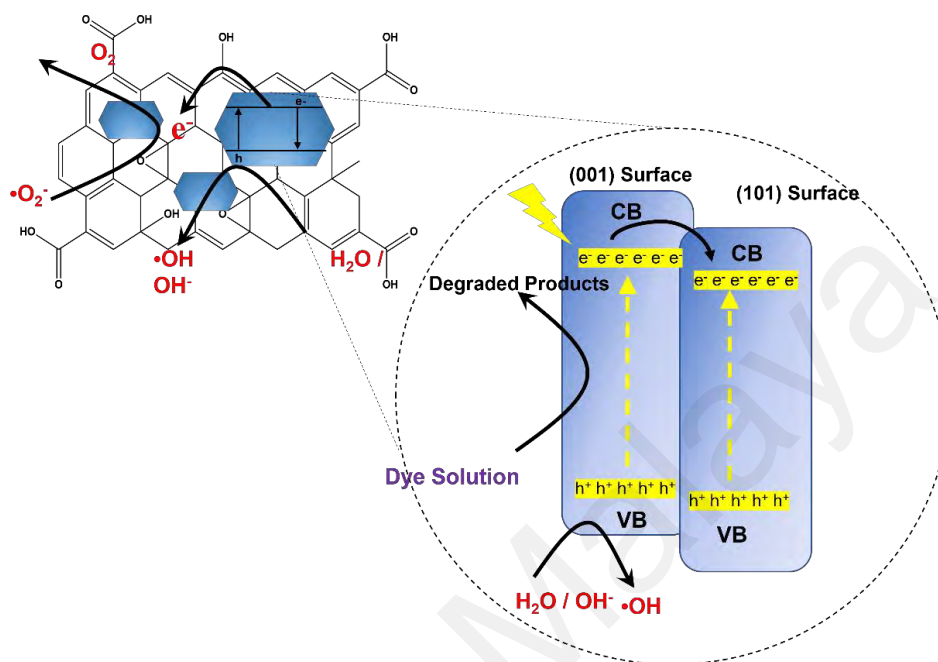
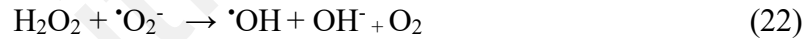


**Figure 4. 13: Proposed energy band diagram mechanism for photocatalytic degradation of TiO<sub>2</sub> (001)/GO nanocomposite dyes.**

Figure 4.13 depicts the potential photodegradation mechanism of TiO<sub>2</sub> (001)/GO nanocomposite as a photocatalyst. Gaseous oxygen and water play an essential role in the photocatalytic degradation reaction. When light radiation impacts the photocatalyst, electrons (e<sup>-</sup>) in the valence band (VB) of TiO<sub>2</sub> are excited to the conduction band (CB), producing holes (h<sup>+</sup>) in the valence band (Equation 18). When photon energy from radiation is equal to or greater than the band gap (E<sub>g</sub>), an electron-hole pair is formed. Additionally, charge carriers can migrate to the surface of the semiconductor or undergo recombination. In the presence of GO, the recombination of electrons and holes is inhibited for enhanced photocatalysis. When agitated electrons interact with adsorbed O<sub>2</sub> molecules, superoxide radicals (•O<sub>2</sub><sup>-</sup>) are produced (Equation 19). These radicals combine with H<sup>+</sup> species to form peroxide molecules or become •OH radicals (Equations 20–22).

Simultaneously, the interaction between H<sub>2</sub>O and OH molecules and holes in the valence band can form an additional •OH radical, as Equations 23–24 demonstrated. In addition, it has been observed that dyes can interact with radical compounds or holes directly or indirectly, leading to the formation of intermediate compounds. These intermediate compounds can subsequently undergo degradation, producing final products such as carbon dioxide and water, as demonstrated in equations 24–26. The following reaction commonly represents the photocatalysis mechanism:



As per the proposed photocatalytic mechanism, several crucial features are involved in the photocatalytic degradation process of TiO<sub>2</sub> (001)/GO nanocomposite. According to reports, graphene oxide (GO) can potentially serve as a charge acceptor due to its two-dimensional planar structure featuring -conjugated bonds. The transfer of photogenerated electrons from TiO<sub>2</sub> (001) to GO is advantageous from an energetic standpoint since the

conduction band of  $\text{TiO}_2$  is more detrimental than the work function of GO. The utilization of GO has the potential to impede charge recombination, thereby increasing the number of charge carriers available to enhance the efficacy of performance degradation. Moreover, the presence of  $\pi$ -conjugated bonds in graphene oxide facilitates its capacity to interact directly with organic dyes, owing to its abundant electron characteristics. The polyaromatic electron system in graphene oxide exhibits a high propensity to interact with the aromatic rings of organic dyes in aqueous media via stacking interactions.

Universiti Malaysia



## CHAPTER 5: CONCLUSIONS

In summary, this study successfully synthesized graphene oxide (GO) from graphite flakes using the modified Hummer method and TiO<sub>2</sub> (001) via the solvothermal method, integrating them with TiO<sub>2</sub> P25 to enhance their photocatalytic activity. Characterization through FTIR, XRD, Raman, and TEM spectroscopy provided detailed insights into the functional groups and properties of the five photocatalysts. Analysis revealed that the band gap energy of TiO<sub>2</sub> (001)/GO was significantly reduced compared to TiO<sub>2</sub> (001) alone, leading to enhanced photocatalytic activity and an expanded visible-light photoactive area. Spectroscopic examinations confirmed that GO/TiO<sub>2</sub> (001) exhibited the highest photocatalytic activity for individual dye components and mixed dye solutions. Remarkably, the degradation efficiency of methylene blue, rhodamine b, crystal violet, and mixed dyes using TiO<sub>2</sub> (001)/GO was determined to be 95%, 92%, 94%, and 87%, respectively. These findings underscore the potential of GO/TiO<sub>2</sub> (001) nanocomposites as effective photocatalysts for wastewater treatment, offering promising prospects for addressing dye pollution challenges.

## REFERENCES

- Abu Hurayra–Lizu, K. M., Bari, M. W., Gulshan, F., & Islam, M. R. (2021). GO based PVA nanocomposites: tailoring of optical and structural properties of PVA with low percentage of GO nanofillers. *Heliyon*, 7(5), e06983. <https://doi.org/10.1016/j.heliyon.2021.e06983>
- Adormaa, B. B., Darkwah, W. K., & Ao, Y. (2018). Oxygen vacancies of the TiO<sub>2</sub> nano-based composite photocatalysts in visible light responsive photocatalysis. *RSC Advances*, 8(58), 33551–33563. <https://doi.org/10.1039/c8ra05117h>
- Ahmed, A. S., Ahamad, T., Ahmad, N., & Khan, M. Z. (2019). Removal enhancement of acid navy blue dye by GO - TiO<sub>2</sub> nanocomposites synthesized using sonication method. *Materials Chemistry and Physics*, 238(July), 121906. <https://doi.org/10.1016/j.matchemphys.2019.121906>
- Ali, A. E., Chowdhury, Z. Z., Devnath, R., Ahmed, M. M., Rahman, M. M., Khalid, K., Wahab, Y. A., Badruddin, I. A., Kamangar, S., Hussien, M., Pallan, K. H., & Mitra, A. (2023). Removal of Azo Dyes from Aqueous Effluent Using Bio-Based Activated Carbons: Toxicity Aspects and Environmental Impact. *Separations*, 10(9). <https://doi.org/10.3390/separations10090506>
- Araujo-Lopez, E., Varilla, L. A., Seriani, N., & Montoya, J. A. (2016). TiO<sub>2</sub> anatase's bulk and (001) surface, structural and electronic properties: A DFT study on the importance of Hubbard and van der Waals contributions. *Surface Science*, 653, 187–196. <https://doi.org/10.1016/j.susc.2016.07.003>
- Arshad, R., Bokhari, T. H., Javed, T., Bhatti, I. A., Rasheed, S., Iqbal, M., Nazir, A., Naz, S., Khan, M. I., Khosa, M. K. K., Iqbal, M., & Zia-ur-Rehman, M. (2020). Degradation product distribution of Reactive Red-147 dye treated by UV/H<sub>2</sub>O<sub>2</sub>/TiO<sub>2</sub> advanced oxidation process. *Journal of Materials Research and Technology*, 9(3), 3168–3178. <https://doi.org/https://doi.org/10.1016/j.jmrt.2020.01.062>
- Balasubramanian, G., Dionysiou, D. D., Suidan, M. T., Baudin, I., & Laîné, J.-M. (2004). Evaluating the activities of immobilized TiO<sub>2</sub> powder films for the photocatalytic degradation of organic contaminants in water. *Applied Catalysis B: Environmental*, 47(2), 73–84. <https://doi.org/https://doi.org/10.1016/j.apcatb.2003.04.002>
- Costinas, C., Salagean, C. A., Cotet, L. C., Baia, M., Todea, M., Magyari, K., & Baia, L. (2022). Insights into the Stability of Graphene Oxide Aqueous Dispersions. In *Nanomaterials* (Vol. 12, Issue 24). <https://doi.org/10.3390/nano12244489>
- Dai, S., Wu, Y., Sakai, T., Du, Z., Sakai, H., & Abe, M. (2010). Preparation of Highly Crystalline TiO<sub>2</sub> Nanostructures by Acid-assisted Hydrothermal Treatment of Hexagonal-structured Nanocrystalline Titania/Cetyltrimethylammonium Bromide Nanoskeleton. *Nanoscale Research Letters*, 5(11), 1829. <https://doi.org/10.1007/s11671-010-9720-0>
- Gao, B., Yuan, X., Lu, P., Lin, B., & Chen, Y. (2015). Enhanced visible-light-driven photocatalytic H<sub>2</sub>-production activity of CdS-loaded TiO<sub>2</sub> microspheres with exposed

- (001) facets. *Journal of Physics and Chemistry of Solids*, 87, 171–176.  
<https://doi.org/10.1016/j.jpccs.2015.08.018>
- Ghasemi, A. (2022). Chapter 7 - Nanoferrite photocatalysts. In A. B. T.-M. F. and R. N. Ghasemi (Ed.), *Micro and Nano Technologies* (pp. 521–585). Elsevier.  
<https://doi.org/https://doi.org/10.1016/B978-0-12-824014-4.00006-8>
- Giovannetti, R., Rommozzi, E., Zannotti, M., & D'Amato, C. (2017). Recent Advances in Graphene Based TiO<sub>2</sub> Nanocomposites (GTiO<sub>2</sub>Ns) for Photocatalytic Degradation of Synthetic Dyes. *Catalysts*, 7, 305. <https://doi.org/10.3390/catal7100305>
- Grätzel, M. (2001). Photoelectrochemical cells. *Nature*, 414(6861), 338–344.  
<https://doi.org/10.1038/35104607>
- Guo, C., Shi, Y., Lu, S., Yu, Y., & Zhang, B. (2021). Amorphous nanomaterials in electrocatalytic water splitting. *Chinese Journal of Catalysis*, 42(8), 1287–1296.  
[https://doi.org/10.1016/S1872-2067\(20\)63740-8](https://doi.org/10.1016/S1872-2067(20)63740-8)
- Guo, Q., Zhou, C., Ma, Z., & Yang, X. (2019). Fundamentals of TiO<sub>2</sub> Photocatalysis: Concepts, Mechanisms, and Challenges. *Advanced Materials*, 31(50), 1–26.  
<https://doi.org/10.1002/adma.201901997>
- Jíříčková, A., Jankovský, O., Sofer, Z., & Sedmidubský, D. (2022). Synthesis and Applications of Graphene Oxide. *Materials*, 15(3).  
<https://doi.org/10.3390/ma15030920>
- Kaushal, A., Dhawan, S. K., & Singh, V. (2019). Determination of crystallite size, number of graphene layers and defect density of graphene oxide (GO) and reduced graphene oxide (RGO). *AIP Conference Proceedings*, 2115(July), 1–5.  
<https://doi.org/10.1063/1.5112945>
- Khalil, M., Pratama, R. I., Sujak, M., Garry, A., Djuhana, D., Umar, A., Lai, C. W., & Jan, B. M. (2020). Dependence of the photocatalytic reduction of bicarbonate to formic acid by Au–TiO<sub>2</sub> on Au morphology and its plasmonic vibrational mode. *Materials Chemistry and Physics*, 249, 123018.  
<https://doi.org/https://doi.org/10.1016/j.matchemphys.2020.123018>
- Khan, S. A., Arshad, Z., Shahid, S., Arshad, I., Rizwan, K., Sher, M., & Fatima, U. (2019). Synthesis of TiO<sub>2</sub>/Graphene oxide nanocomposites for their enhanced photocatalytic activity against methylene blue dye and ciprofloxacin. *Composites Part B: Engineering*, 175(June), 107120. <https://doi.org/10.1016/j.compositesb.2019.107120>
- Khannam, M., Sharma, S., Dolui, S., & Dolui, S. K. (2016). A graphene oxide incorporated TiO<sub>2</sub> photoanode for high efficiency quasi solid state dye sensitized solar cells based on a poly-vinyl alcohol gel electrolyte. *RSC Advances*, 6(60), 55406–55414.  
<https://doi.org/10.1039/c6ra07577k>
- Köppen, S., & Langel, W. (2008). Adsorption of small organic molecules on anatase and rutile surfaces: a theoretical study. *Physical Chemistry Chemical Physics*, 10(14), 1907–1915. <https://doi.org/10.1039/B719098K>
- Kusiak-nejman, E., & Morawski, A. W. (2019). Applied Catalysis B : Environmental TiO<sub>2</sub> / graphene-based nanocomposites for water treatment : A brief overview of charge carrier transfer , antimicrobial and photocatalytic performance. *Applied Catalysis B:*

- Environmental*, 253(April), 179–186. <https://doi.org/10.1016/j.apcatb.2019.04.055>
- Lee, T.-Y., Lee, C.-Y., & Chiu, H.-T. (2018). Enhanced Photocatalysis from Truncated Octahedral Bipyramids of Anatase TiO<sub>2</sub> with Exposed {001}/{101} Facets. *ACS Omega*, 3(8), 10225–10232. <https://doi.org/10.1021/acsomega.8b01251>
- Lellis, B., Fávaro-Polonio, C. Z., Pamphile, J. A., & Polonio, J. C. (2019). Effects of textile dyes on health and the environment and bioremediation potential of living organisms. *Biotechnology Research and Innovation*, 3(2), 275–290. <https://doi.org/https://doi.org/10.1016/j.biori.2019.09.001>
- Li, S., Lin, Q., Liu, X., Yang, L., Ding, J., Dong, F., Li, Y., Irfan, M., & Zhang, P. (2018). Fast photocatalytic degradation of dyes using low-power laser-fabricated Cu<sub>2</sub>O–Cu nanocomposites. *RSC Advances*, 8, 20277–20286. <https://doi.org/10.1039/C8RA03117G>
- Lin, C., Gao, Y., Zhang, J., Xue, D., Fang, H., Tian, J., Zhou, C., Zhang, C., Li, Y., & Li, H. (2020). GO/TiO<sub>2</sub> composites as a highly active photocatalyst for the degradation of methyl orange. *Journal of Materials Research*, 35(10), 1307–1315. <https://doi.org/10.1557/jmr.2020.41>
- Liu, B., Huang, Y., Wen, Y., Du, L., Zeng, W., Shi, Y., Zhang, F., Zhu, G., Xu, X., & Wang, Y. (2012). Highly dispersive {001} facets-exposed nanocrystalline TiO<sub>2</sub> on high quality graphene as a high performance photocatalyst. *Journal of Materials Chemistry*, 22(15), 7484–7491. <https://doi.org/10.1039/C2JM16114A>
- Liu, H., Li, P., Bai, H., Du, C., Wei, D., Su, Y., Wang, Y., & Yang, L. (2018). Incorporation of reduced graphene oxide into faceted flower-like {001} TiO<sub>2</sub> for enhanced photocatalytic activity. *Royal Society Open Science*, 5(8), 180613. <https://doi.org/10.1098/rsos.180613>
- Liu, S., Yu, J., & Jaroniec, M. (2011). Anatase TiO<sub>2</sub> with dominant high-energy {001} facets: Synthesis, properties, and applications. *Chemistry of Materials*, 23(18), 4085–4093. <https://doi.org/10.1021/cm200597m>
- Loryuenyong, V., Totepvimarn, K., Eimburanapratvat, P., Boonchompoo, W., & Buasri, A. (2013). Preparation and Characterization of Reduced Graphene Oxide Sheets via Water-Based Exfoliation and Reduction Methods. *Advances in Materials Science and Engineering*, 2013, 923403. <https://doi.org/10.1155/2013/923403>
- Lu, T., Zhang, R., Hu, C., Chen, F., Duo, S., & Hu, Q. (2013). TiO<sub>2</sub>–graphene composites with exposed {001} facets produced by a one-pot solvothermal approach for high performance photocatalyst. *Physical Chemistry Chemical Physics*, 15(31), 12963–12970. <https://doi.org/10.1039/C3CP50942G>
- Maheshwari, K., Agrawal, M., & Gupta, A. B. (2021). *Dye Pollution in Water and Wastewater BT - Novel Materials for Dye-containing Wastewater Treatment* (S. S. Muthu & A. Khadir (eds.); pp. 1–25). Springer Singapore. [https://doi.org/10.1007/978-981-16-2892-4\\_1](https://doi.org/10.1007/978-981-16-2892-4_1)
- Mani, S., & Bharagava, R. N. (2016). *Exposure to Crystal Violet, Its Toxic, Genotoxic and Carcinogenic Effects on Environment and Its Degradation and Detoxification for Environmental Safety BT - Reviews of Environmental Contamination and Toxicology*

*Volume 237* (W. P. de Voogt (ed.); pp. 71–104). Springer International Publishing.  
[https://doi.org/10.1007/978-3-319-23573-8\\_4](https://doi.org/10.1007/978-3-319-23573-8_4)

- Marcano, D. C., Kosynkin, D. V., Berlin, J. M., Sinitskii, A., Sun, Z., Slesarev, A., Alemany, L. B., Lu, W., & Tour, J. M. (2010). Improved Synthesis of Graphene Oxide. *ACS Nano*, 4(8), 4806–4814. <https://doi.org/10.1021/nn1006368>
- Muzyka, R., Drewniak, S., Pustelny, T., Chrubasik, M., & Gryglewicz, G. (2018). Characterization of graphite oxide and reduced graphene oxide obtained from different graphite precursors and oxidized by different methods using Raman spectroscopy. *Materials*, 11(7), 15–17. <https://doi.org/10.3390/ma11071050>
- Najafi, M., Kermanpur, A., Rahimipour, M. R., & Najafzadeh, A. (2017). Effect of TiO<sub>2</sub> morphology on structure of TiO<sub>2</sub>-graphene oxide nanocomposite synthesized via a one-step hydrothermal method. *Journal of Alloys and Compounds*, 722, 272–277. <https://doi.org/https://doi.org/10.1016/j.jallcom.2017.06.001>
- Oladoye, P. O., Ajiboye, T. O., Omotola, E. O., & Oyewola, O. J. (2022). Methylene blue dye: Toxicity and potential elimination technology from wastewater. *Results in Engineering*, 16, 100678. <https://doi.org/https://doi.org/10.1016/j.rineng.2022.100678>
- Ong, W. J., Tan, L. L., Chai, S. P., Yong, S. T., & Mohamed, A. R. (2014). Highly reactive {001} facets of TiO<sub>2</sub>-based composites: Synthesis, formation mechanism and characterization. *Nanoscale*, 6(4), 1946–2008. <https://doi.org/10.1039/c3nr04655a>
- Oshani, F., Marandi, R., Rasouli, S., & Farhoud, M. K. (2014). Photocatalytic investigations of TiO<sub>2</sub>-P25 nanocomposite thin films prepared by peroxotitanic acid modified sol-gel method. *Applied Surface Science*, 311, 308–313. <https://doi.org/https://doi.org/10.1016/j.apsusc.2014.05.059>
- Oshida, Y. (2013). *4 - Oxidation and Oxides* (Y. B. T.-B. and B. of T. M. (Second E. Oshida (ed.); pp. 87–115). Elsevier. <https://doi.org/https://doi.org/10.1016/B978-0-444-62625-7.00004-2>
- Oyekanmi, A. A., Ahmad, A., Hossain, K., & Rafatullah, M. (2019). Adsorption of Rhodamine B dye from aqueous solution onto acid treated banana peel: Response surface methodology, kinetics and isotherm studies. *PLOS ONE*, 14(5), e0216878. <https://doi.org/10.1371/journal.pone.0216878>
- Pakade, V., Cukrowska, E., Darkwa, J., Torto, N., & Chimuka, L. (2011). Selective removal of chromium (VI) from sulphates and other metal anions using an ion-imprinted polymer. *Water SA*, 37(4), 529–538. <https://doi.org/10.4314/wsa.v37i4.11>
- Qianqian, Z., Tang, B., & Guoxin, H. (2011). High photoactive and visible-light responsive graphene/titanate nanotubes photocatalysts: Preparation and characterization. *Journal of Hazardous Materials*, 198, 78–86. <https://doi.org/https://doi.org/10.1016/j.jhazmat.2011.10.012>
- Ramos, D. K. C., González, M. V., Muñoz, R. A. E., Cruz, J. S., De Moure-Flores, F. J., & Mayén-Hernández, S. A. (2020). Obtaining and Characterization of TiO<sub>2</sub>-GO Composites for Photocatalytic Applications. *International Journal of Photoenergy*, 2020, 3489218. <https://doi.org/10.1155/2020/3489218>
- REHMAN, F., MURTAZA, S., ALI KHAN, J., & KHAN, H. M. (2017). REMOVAL OF

CRYSTAL VIOLET DYE FROM AQUEOUS SOLUTION BY GAMMA IRRADIATION. *Journal of the Chilean Chemical Society*, 62, 3359–3364. [http://www.scielo.cl/scielo.php?script=sci\\_arttext&pid=S0717-97072017000100011&nrm=iso](http://www.scielo.cl/scielo.php?script=sci_arttext&pid=S0717-97072017000100011&nrm=iso)

- Saeed, M., Muneer, M., Haq, A. ul, & Akram, N. (2022). Photocatalysis: an effective tool for photodegradation of dyes—a review. *Environmental Science and Pollution Research*, 29(1), 293–311. <https://doi.org/10.1007/s11356-021-16389-7>
- Sajan, C. P., Wageh, S., Al-Ghamdi, A. A., Yu, J., & Cao, S. (2016). TiO<sub>2</sub> nanosheets with exposed {001} facets for photocatalytic applications. *Nano Research*, 9(1), 3–27. <https://doi.org/10.1007/s12274-015-0919-3>
- Samchetshabam, G., Hussan Ajmal, & Choudhury. T. G. (2017). Impact of textile dyes waste on aquatic environments and its treatment. *Environ. Ecol*, 35(3C), pp.2349-2353. *Environment & Ecology*, 35(3C), 2349-2353.
- Sanjaya, A. R., Amanda, S., Ivandini, T. A., Abnisa, F., Kadja, G. T. M., Pratomo, U., Alias, Y., & Khalil, M. (2023). Fabrication of Graphene Oxide-Decorated Mesoporous NiFe<sub>2</sub>O<sub>4</sub> as an Electrocatalyst in the Hydrogen Gas Evolution Reaction. *Designs*, 7(1), 1–12. <https://doi.org/10.3390/designs7010026>
- Schneider, J., Matsuoka, M., Takeuchi, M., Zhang, J., Horiuchi, Y., Anpo, M., & Bahnemann, D. W. (2014). Understanding TiO<sub>2</sub> Photocatalysis: Mechanisms and Materials. *Chemical Reviews*, 114(19), 9919–9986. <https://doi.org/10.1021/cr5001892>
- Sharif, A. (2020). Microbial degradation of textile industry effluents: A review. *Pure and Applied Biology*, 9(4), 2361–2382. <https://doi.org/10.19045/bspab.2020.90251>
- Sharma, M., Behl, K., Nigam, S., & Joshi, M. (2018). TiO<sub>2</sub>-GO nanocomposite for photocatalysis and environmental applications: A green synthesis approach. *Vacuum*, 156(December 2017), 434–439. <https://doi.org/10.1016/j.vacuum.2018.08.009>
- Shen, Y., Saeki, A., Seki, S., Lee, J.-O., Aimi, J., & Nakanishi, T. (2015). Exfoliation of Graphene and Assembly Formation with Alkylated-C60: A Nanocarbon Hybrid towards Photo-Energy Conversion Electrode Devices. *Advanced Optical Materials*, 3(7), 925–930. <https://doi.org/https://doi.org/10.1002/adom.201400619>
- Sinar Mashuri, S. I., Ibrahim, M. L., Kasim, M. F., Mastuli, M. S., Rashid, U., Abdullah, A. H., Islam, A., Asikin Mijan, N., Tan, Y. H., Mansir, N., Mohd Kaus, N. H., & Yun Hin, T.-Y. (2020). Photocatalysis for Organic Wastewater Treatment: From the Basis to Current Challenges for Society. In *Catalysts* (Vol. 10, Issue 11). <https://doi.org/10.3390/catal10111260>
- Singh, E., & Nalwa, H. S. (2015). Graphene-Based Dye-Sensitized Solar Cells: A Review. *Science of Advanced Materials*, 9, 1863–1912. <https://doi.org/10.1166/sam.2015.2438>
- Singh, P., Shandilya, P., Raizada, P., Sudhaik, A., Rahmani-Sani, A., & Hosseini-Bandegharai, A. (2020). Review on various strategies for enhancing photocatalytic activity of graphene based nanocomposites for water purification. *Arabian Journal of Chemistry*, 13(1), 3498–3520. <https://doi.org/https://doi.org/10.1016/j.arabjc.2018.12.001>
- Smithson, J., & Mitchell, P. B. (2019). Chapter 2 - Antidepressants. In S. D. B. T.-S. E. of

- D. A. Ray (Ed.), *A Worldwide Yearly Survey of New Data in Adverse Drug Reactions* (Vol. 41, pp. 13–26). Elsevier.  
<https://doi.org/https://doi.org/10.1016/bs.seda.2019.10.002>
- Su, C., Hong, B.-Y., & Tseng, C.-M. (2004). Sol–gel preparation and photocatalysis of titanium dioxide. *Catalysis Today*, *96*(3), 119–126.  
<https://doi.org/https://doi.org/10.1016/j.cattod.2004.06.132>
- Sulistina, D. R., & Martini, S. (2020). The Effect of Rhodamine B on the Cerebellum and Brainstem Tissue of Rattus Norvegicus. *Journal of Public Health Research*, *9*(2), jphr.2020.1812. <https://doi.org/10.4081/jphr.2020.1812>
- Tang, J., Zou, Z., Yin, J., & Ye, J. (2003). Photocatalytic degradation of methylene blue on CaIn<sub>2</sub>O<sub>4</sub> under visible light irradiation. *Chemical Physics Letters*, *382*(1–2), 175–179. <https://doi.org/10.1016/j.cplett.2003.10.062>
- Tayel, A., Ramadan, A. R., & El Seoud, O. A. (2018). Titanium Dioxide/Graphene and Titanium Dioxide/Graphene Oxide Nanocomposites: Synthesis, Characterization and Photocatalytic Applications for Water Decontamination. In *Catalysts* (Vol. 8, Issue 11). <https://doi.org/10.3390/catal8110491>
- Tian, F., Zhang, Y., Zhang, J., & Pan, C. (2012). Raman Spectroscopy: A New Approach to Measure the Percentage of Anatase TiO<sub>2</sub> Exposed {001} Facets. *The Journal of Physical Chemistry C*, *116*(13), 7515–7519. <https://doi.org/10.1021/jp301256h>
- Völz, H. G., Kischkewitz, J., Woditsch, P., Westerhaus, A., Griebler, W.-D., De Liedekerke, M., Buxbaum, G., Printzen, H., Mansmann, M., Råde, D., Trenczek, G., Wilhelm, V., Schwarz, S., Wienand, H., Adel, J., Adrian, G., Brandt, K., Cork, W. B., Winkeler, H., ... Gaedcke, H. (2006). Pigments, Inorganic. In *Ullmann's Encyclopedia of Industrial Chemistry*.  
[https://doi.org/https://doi.org/10.1002/14356007.a20\\_243.pub2](https://doi.org/https://doi.org/10.1002/14356007.a20_243.pub2)
- Wang, W.-S., Wang, D.-H., Qu, W.-G., Lu, L.-Q., & Xu, A.-W. (2012). Large Ultrathin Anatase TiO<sub>2</sub> Nanosheets with Exposed {001} Facets on Graphene for Enhanced Visible Light Photocatalytic Activity. *The Journal of Physical Chemistry C*, *116*(37), 19893–19901. <https://doi.org/10.1021/jp306498b>
- Xu, J., He, Q., Xiong, Z., Yu, Y., Zhang, S., Hu, X., Jiang, L., Su, S., Hu, S., Wang, Y., & Xiang, J. (2021). Raman spectroscopy as a versatile tool for investigating thermochemical processing of coal, biomass, and wastes: Recent advances and future perspectives. *Energy and Fuels*, *35*(4), 2870–2913.  
<https://doi.org/10.1021/acs.energyfuels.0c03298>
- Yang, H. G., Sun, C. H., Qiao, S. Z., Zou, J., Liu, G., Smith, S. C., Cheng, H. M., & Lu, G. Q. (2008). Anatase TiO<sub>2</sub> single crystals with a large percentage of reactive facets. *Nature*, *453*(7195), 638–641. <https://doi.org/10.1038/nature06964>
- Ye, L., Mao, J., Liu, J., Jiang, Z., Peng, T., & Zan, L. (2013). Synthesis of anatase TiO<sub>2</sub> nanocrystals with {101}, {001} or {010} single facets of 90% level exposure and liquid-phase photocatalytic reduction and oxidation activity orders. *Journal of Materials Chemistry A*, *1*(35), 10532–10537. <https://doi.org/10.1039/C3TA11791J>
- Yunarti, R. T., Safitri, T. N., Dimonti, L. C. C., Aulia, G., Khalil, M., & Ridwan, M.

- (2022). Facile synthesis of composite between titania nanoparticles with highly exposed (001) facet and coconut shell-derived graphene oxide for photodegradation of methylene blue. *Journal of Physics and Chemistry of Solids*, 160, 110357. <https://doi.org/https://doi.org/10.1016/j.jpcs.2021.110357>
- Zhang, H., Wang, X., Li, N., Xia, J., Meng, Q., Ding, J., & Lu, J. (2018). Synthesis and characterization of TiO<sub>2</sub>/graphene oxide nanocomposites for photoreduction of heavy metal ions in reverse osmosis concentrate. *RSC Advances*, 8(60), 34241–34251. <https://doi.org/10.1039/C8RA06681G>
- Zhao, D., Sheng, G., Chen, C., & Wang, X. (2012). Enhanced photocatalytic degradation of methylene blue under visible irradiation on graphene@TiO<sub>2</sub> dyade structure. *Applied Catalysis B: Environmental*, 111–112, 303–308. <https://doi.org/10.1016/j.apcatb.2011.10.012>
- Zhong, Q., Vohs, J. M., & Bonnell, D. A. (1992). Effect of reduction on the topographic and electronic structure of TiO<sub>2</sub>(110) surfaces. *Surface Science*, 274(1), 35–43. [https://doi.org/https://doi.org/10.1016/0039-6028\(92\)90097-P](https://doi.org/https://doi.org/10.1016/0039-6028(92)90097-P)
- Zhou, X., Zhang, X., Wang, Y., & Wu, Z. (2021). 2D Graphene-TiO<sub>2</sub> Composite and Its Photocatalytic Application in Water Pollutants. *Frontiers in Energy Research*, 8(February), 1–10. <https://doi.org/10.3389/fenrg.2020.612512>
- Zhu, J., Liu, Z., Yang, F., Long, D., Jian, Y., & Pu, S. (2022). The Preparation of {001} TiO<sub>2</sub>/TiOF<sub>2</sub> via a One-Step Hydrothermal Method and Its Degradation Mechanism of Ammonia Nitrogen. *Materials*, 15(18), 1–16. <https://doi.org/10.3390/ma15186465>